FLUORESCENT GOLD ION SENSORS: DESIGN, SYNTHESIS AND IMAGING

A Thesis Submitted to
the Graduate School of Engineering and Sciences of
İzmir Institute of Technology
in Partial Fulfillment of the Requirements for the Degree of

MASTER OF SCIENCE

in Chemistry

by

Beraat Umur KAYA

December 2021
İZMİR

ACKNOWLEDGMENTS

I would like to express my appreciation to all people in my life for their support and patience, in particular to Prof. Dr. Mustafa Emrullahoğlu for recruiting me to his research group while I was taking my undergraduate education and giving me the chance to continue to chase my dreams for three years of master's degree education. It was an honor for me to have him as a mentor who has his guidance, support, encouragement, and belief.

I would like to thank to Scientific and Technical Research Council of Turkey for financial support for this project (118Z418). I am grateful to all members of Emrullahoğlu Research Group, Buse Tütüncü, Miray Cebeci, Ahmet Eren, Ezgi Vural, and especially to Suay Dartar for her endless help during my studies.

I am very thankful to my committee members, Prof. Dr. Mehtap Eanes and Assos. Prof. Dr. Murat Işık for their precious time and support.

I would like to thank my mother Leman Kaya and my father Adem Kaya for their support. I am deeply grateful to all my friends especially to Hande İpek Yamanel, Ali Coşar, Berk Yazıcı, Çağlar Kocavardar, Seher and İlyas Balcı, and Ali Tümbet for being as close as siblings can be. I would also like to thank my friends from IZTECH; Mert Korkutan, Hakan Berk Aydın, Devrim Bulsoy, Yankı Öncü Yayak, Emre Karaburun, and Alper Şahin for making life in IZTECH endurable. Moreover, I am thankful to my friends; Çağdaş Adıören, Elif Polat, Halil Yıldırım, Mert Kayral and Yiğit Şahin for their valuable and enjoyable friendship.

I am deeply and forever indebted to Ezgi Vural, my friend, my co-worker and my love, for holding me every time I fall down. Thank you for making everything much more easier with your everlasting encouragement and invaluable support. Lastly, I am grateful to have Luke, our cat, in my life for always jumping to my keyboard while I was writing this thesis.

ABSTRACT

FLUORESCENT GOLD ION SENSORS: DESIGN, SYNTHESIS AND IMAGING

Of all transition metals, gold has long sustained attention owing to its unique chemical and physical properties. Beyond that, the ease of processing gold allows its use in science, industry, and in various chemical, biological, and medical applications. For example, gold is used in medicine to treat rheumatoid arthritis, asthma, cancer, and brain and skin lesions. However, the extensive use of gold compounds can adversely impact the natural environment and biological systems due to their potential toxicity. For those reasons, identifying trace amounts of gold species in solution and cell media is crucial.

Unlike the detection methods of atomic absorption spectroscopy, atomic emission spectroscopy, and inductively coupled plasma spectrometry, fluorescence-based detection methods offer easy sample preparation, rapid response, high sensitivity, reproducibility, and efficiency, all at a low cost. Today, various types of fluorescent sensors selective to gold ions have been designed, typically with BODIPY, fluorescein, rhodamine, naphthalimide, and coumarin-based fluorophores.

In the work for this thesis, for the first time an enyne-derived BODIPY-based sensor was designed and synthesised to identify Au^{3+} ions, after which photophysical changes in the presence and absence of the analyte were examined both in solutions and in cells.

ÖZET

FLORESAN ALTIN İYON ALGILAYICILARI: TASARIM, SENTEZ VE GÖRÜNTÜLEME

Diğer geçiş metalleri arasında altın, benzersiz kimyasal ve fiziksel özellikleri nedeniyle insanları cezbetmektedir. Altın metalinin kolay işlenebilirliği, bilim, endüstri, kimya, biyolojik ve çeşitli tıbbi uygulamalarda kullanılmasına izin verir. Buna örnek olarak altın tıp alanında Romatoid artrit, astım, tüberküloz, sıtma, kanser, HIV ve beyin lezyonları gibi çeşitli hastalıkların tedavisinde kullanılmaktadır. Ancak, altın iyonlarının yaygın kullanımı, potansiyel toksititesi nedeniyle doğa ve biyolojik sistemler üzerinde çeşitli olumsuz etkilere sahiptir. Bu sebeplerden dolayı, altın bileşiklerinin çözelti ve hücre ortamlarında eser miktarlarda tayini oldukça önemlidir.

Atomik absorpsiyon ve atomik emisyon spektroskopisi, indüktif eşleşmiş plazma spektrometresi gibi farklı tespit yöntemlerine karşılık floresan algılama yöntemleri, basit örnek hazırlama, hızlı yanıt süresi, düşük maliyeti, yüksek hassasiyet, tekrarlanabilirlik, ve verimlilik konularında üstün olmuştur. Günümüzde, altın iyonlarına seçici olan çeşitli floresan sensör algılayıcıları tasarlanmıştır. BODIPY, floresein, rodamin, naftalimid ve kumarin bazlı floroforlar, altın iyon algılayıcı floresan probların tasarımında çok yaygındır.

Bu tez çalışmasında, Au^{3+} iyonlarının tayini için literatürde daha önce hiç kullanılmamış enyne motifi ile türevlendirilmiş BODIPY tabanlı algılayıcının tasarlanması, sentezlenmesi ve hem çözeltilerde hem de hücre içerisindeki analit varlığında ve yokluğunda fotofiziksel değişimlerinin incenlemesi amaçlanmıştır.

TABLE OF CONTENTS

LIST OF FIGURES

Figure **Page**

Figure **Page**

LIST OF ABBREVIATIONS

ICP-OES	Inductively coupled plasma optical-emission spectroscopy
ICP-AES	Inductively coupled plasma atomic-emission spectroscopy
ICP-MS	Inductively coupled plasma mass spectroscopy
PET	Photo-induced electron transfer
FRET	Fluorescence resonance energy transfer
ICT	Intramolecular charge transfer
TBET	Through-bond energy transfer
CHEF	Chelation enhanced fluorescence
TICT	Twisted intramolecular/intermediate charge transfer
PICT	Planar intramolecular charge transfer
HOMO	Highest occupied molecular orbital
LUMO	Lowest unoccupied molecular orbital
BODIPY	4,4-difluoro-4-bora-3a,4a-diaza-s-indacene
DDQ	2,3-dichloro-5,6-dicyano-1,4-benzoquinone
EtOH	Ethanol
HEPES	4-(2-Hydroxyethyl)piperazine-1-ethanesulfonic acid
CH_3CN	Acetonitrile
PBS	Phosphate-buffered saline
MeOH	Methanol
$CDCl_3$	Deuterated chloroform
FBS	Fetal bovine serum
DAPI	4′,6-diamidino-2-phenylindole
HI	Hydrogen iodide
TMSCl	Trimethylsilyl chloride
DCM	Dichloromethane
DMF	Dimethylformamide

CHAPTER 1

INTRODUCTION

1.1. An Overview

Transition metals (e.g. Au, Ag, and Pd) have long played essential roles in human life. Owing to their unique chemical and physical properties, they have been used in science, industry, and various medical applications(She et al. 2021). Among them, gold has consistently attracted attention due to not only due its bright, shiny appearance but also its malleable nature and unique chemical properties that allow its ions to be used in both chemical and biological applications (Singha et al. 2015).

In recent decades, gold species have been used to catalyse chemical reactions and to activate C-C multiple bonds, and that ability has served as an essential criterion for gold-catalysed organic reactions primarily for alkynes (Hashmi and Rudolph 2008). With the lowest electrochemical potential of all metallic elements, gold has a strong Lewis acid character, and its cationic forms therefore readily take electrons from any reductant and convert them to their metallic form, as well as activate alkynes for nucleophilic addition (Laguna 2009). Beyond chemistry, gold has also been used in dentistry as a filling material and in medicine to treat rheumatoid arthritis, asthma, cancer, and brain and skin lesions due to its high biocompatibility (Knosp, Holliday, and Corti 2003) (Sadler and Department 1996). Although gold species can play critical roles in treating diseases, overexposure to gold ions (e.g. Au^{+} and Au^{3+}) can adversely impact the natural environment and biological systems due to their toxicity and relative reactivity. For that reason, the detection of gold ions is crucial (Yuan et al. 2011).

Because gold ions are present in nature in lower amounts than other transition metals, their analysis is usually referred to as trace metal analysis, and many detection methods have been developed to investigate both the side-effects and benefits of gold ions. Of the various detection methods available, including inductively coupled plasma

optical-emission spectroscopy (ICP-OES), inductively coupled plasma atomic-emission spectroscopy (ICP-AES), inductively coupled plasma mass spectroscopy (ICP-MS), fluorescence sensing strategies are superior owing to their simple sample preparation, rapid response , low cost, high sensitivity, reproducibility, and efficiency(Carter, Young, and Palmer 2014)(Singha et al. 2015).

1.2. Fluorescent Chemosensors

Changes in the environment-for instance, in light, heat, motion, and gas leakage-can be detected and converted to readable signals via sensors. In particular, chemosensors consist of two fundamental units: the receptor unit, which interacts with an analyte, and the fluorophore unit, which generates a detectable optical signal. Fluorescent chemosensors can be designed in two ways: either by separating the receptor unit by a spacer or linker (e.g. an alkyl chain) to prevent conjugation or, directly attaching or integrating fluorophore and receptor unit into each other, in which case the receptor unit participates in the fluorophore unit's π-system (Figure 1.1) (Duke et al. 2010).

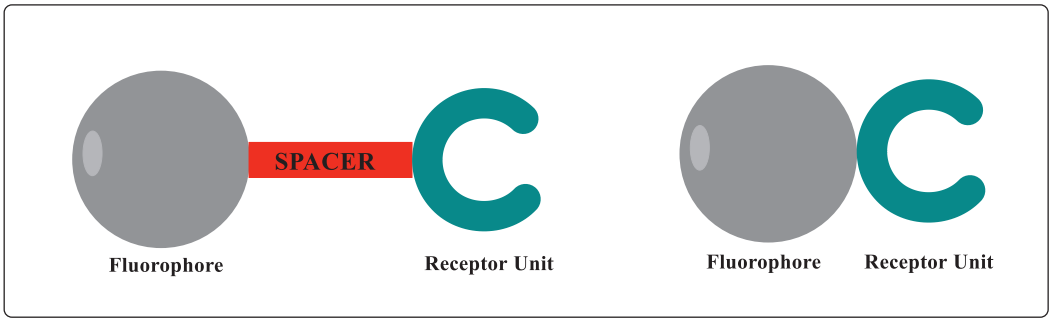

Figure 1.1. Schematic representation of design concept for the construction fluorescent chemosensor
(Source: Duke et al. 2010)

The signal of a fluorescent sensor is formed with a change in the absorbance, fluorescence, or fluorescence lifetimes of the fluorophore unit. The interaction of the

analyte and the receptor unit causes changes in the unit's fluorescence such that the emission wavelength may be shifted, diminished (i.e. turned off), or generated (i.e. turned on) (Figure 1.2) (Cheng, Zhou, and Xiang 2015).

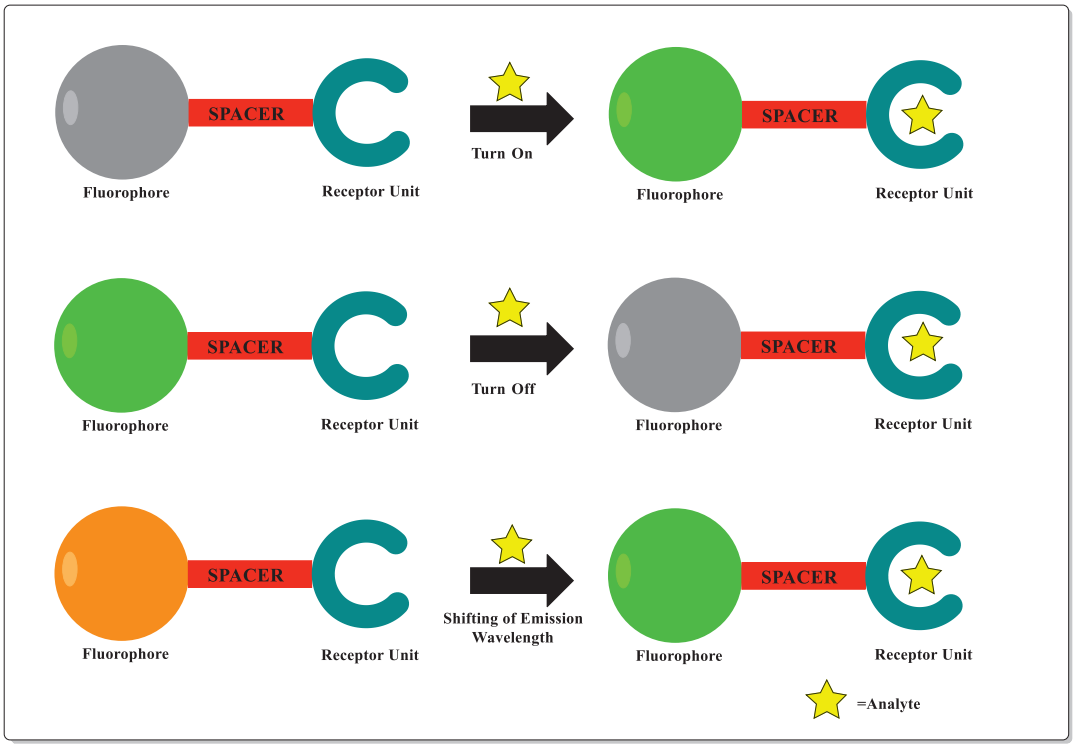

Figure 1.2. Representation of a) Turn on b) Turn off and c) Shifting of emission wavelength

When the analyte interacts with the receptor unit, the photophysical mechanism of the sensor changes, which makes the fluorophore unit's optical properties observable. In designing fluorescent chemosensors to detect metals and amino acids, among other things, the photophysical mechanism can be photo-induced electron transfer (PET), fluorescence resonance energy transfer (FRET), intramolecular charge transfer (ICT), through-bond energy transfer (TBET), chelation enhanced fluorescence (CHEF), twisted intramolecular/intermediate charge transfer (TICT), or planar intramolecular charge transfer (PICT).

1.2.1. Photo-induced Electron Transfer (PET)

Each sensor based on PET usually consists of a receptor unit integrated into a fluorophore unit via a spacer and includes a heteroatom with nonbonding electron pairs (e.g. N, O, S, and P). The highest occupied molecular orbital (HOMO) of the receptor unit lies between the HOMO and lowest unoccupied molecular orbital (LUMO) of the excited fluorophore. Following the excitation of the fluorophore, the electrons in the HOMO of the free receptor are transferred to the HOMO of the excited fluorophore, which causes the quenching of the fluorophore's fluorescent property. When the analyte is coordinated with the lone pair electrons of the receptor unit, its HOMO energy level drops due to the increased redox potential. As a result, PET is blocked, and strong fluorescence emission can be observed (Figure 1.3) (Das, Dutta, and Das 2013).

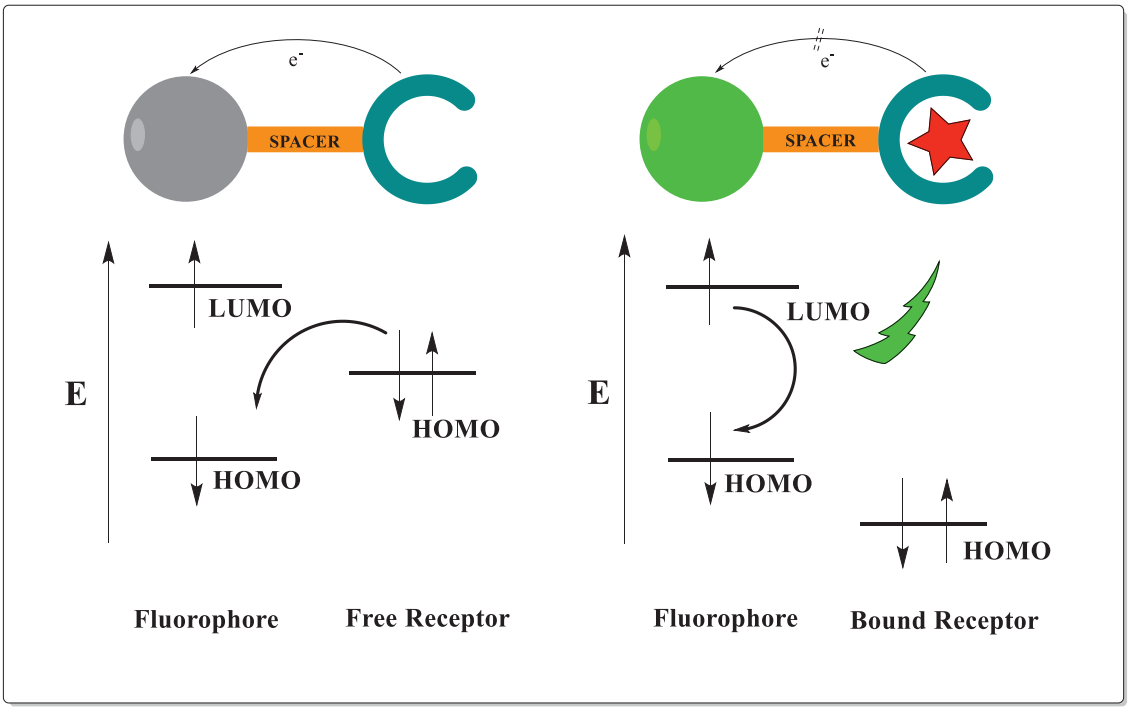

Figure 1.3. Photo-induced electron transfer mechanism
(Source: Das, Dutta, and Das 2013)

Today, various types of fluorescence sensors selective to gold ions have been designed, often with 4,4-difluoro-4-bora-3a,4a-diaza-s-indacene (BODIPY)-based,

fluorescein-based, naphthalimide-based, and coumarin-based fluorophores (Karakuş, Cakan-Akdogan, and Emrullahoglu 2015).

1.3. 4,4-difluoro-4-bora-3a,4a-diaza-s-indacene (BODIPY)

First reported as a fluorophore by Treibs and Kreuzer in 1968, the highly fluorescent BODIPY dye was originally synthesised serendipitously in a reaction of 2,4-dimethylpyrrole, acetic anhydride, and boron trifluoride expected to yield acylated dimethylpyrrole (Figure 1.4) (Treibs and Kreuzer 1968).

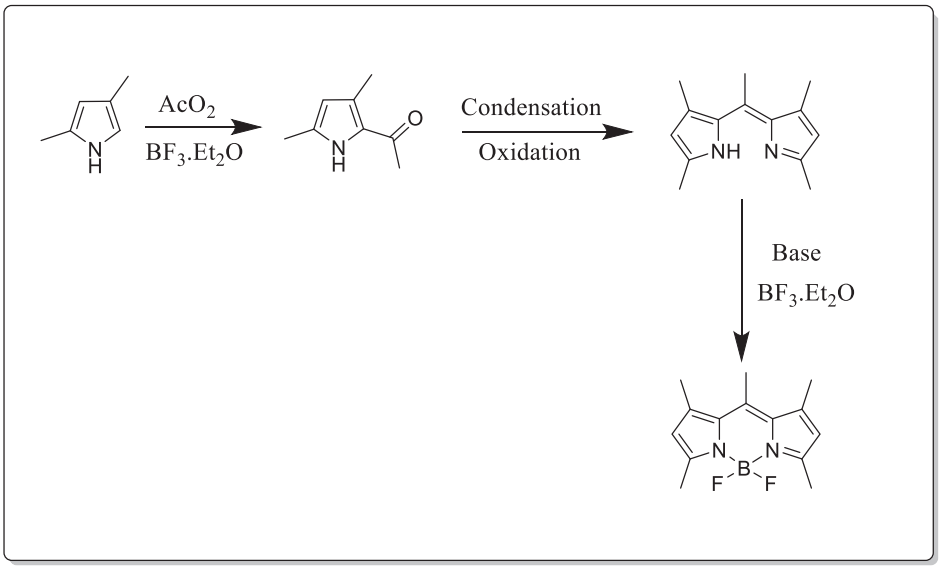

Figure 1.4. Serendipitious discovery of BODIPY
(Source: Treibs and Kreuzer 1968)

Two synthetic pathways are available for obtaining the BODIPY core based on porphyrin chemistry. The first is an acid catalysed condensation reaction of pyrrole and an aldehyde to produce dipyrromethane, which becomes immediately oxidised to dipyrrin by using p-chloranil or 2,3-dichloro-5,6-dicyano-1,4-benzoquinone (DDQ) as an oxidising agent. Unsubstituted dipyrromethane requires excess pyrrole because of its

high sensitivity to light and air. Once dipyrromethane has oxidised, an organic base (e.g. triethylamine and diisopropylamine) and boron trifluoride are added to dipyrrin to obtain the BODIPY core in high yields (Figure 1.5) (Wood and Thompson 2007) (Littler et al. 1999).

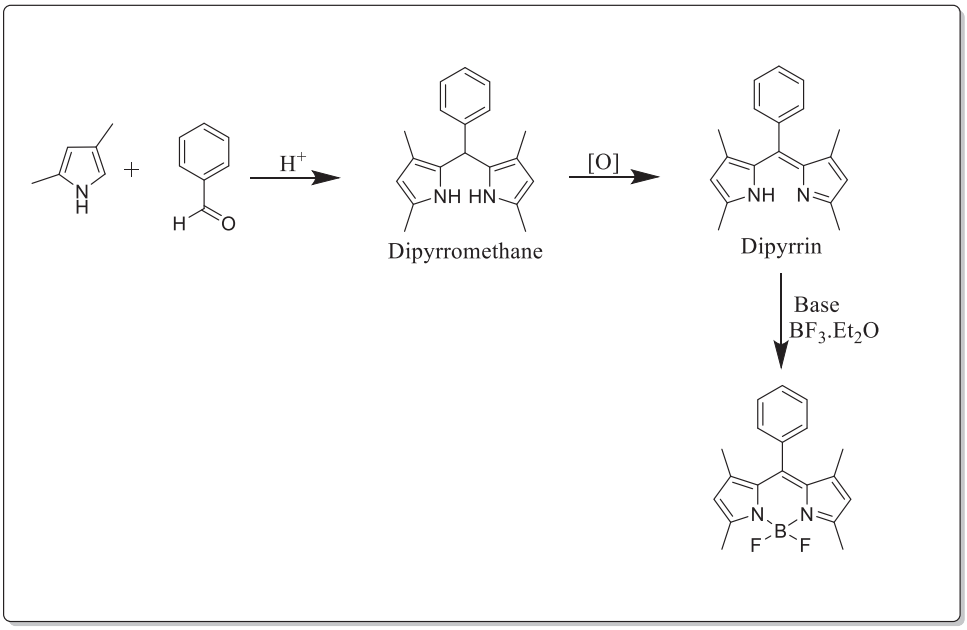

Figure 1.5. Acid catalyzed condensation of aromatic aldehydes with pyrroles (Source: Noel Boens, Leen, and Dehaen 2012)0

The second method requires an acylium derivative instead of an aldehyde. The acylium derivative can be an acid anhydride (Z. Li, Mintzer, and Bittman 2006), an acid halide (Boyer et al. 1993), or an ortho-ester (Yakubovskyi, Shandura, and Kovtun 2009). The reaction between pyrrole and the acylium derivative yields acyl pyrrole as an intermediate. Under acidic conditions, an excess of pyrrole reacts with acyl pyrrole and creates a dipyrrinium salt and thus eliminates the need for an oxidising agent. The salt can easily be converted to BODIPY dye after treatment with an organic base and boron trifluoride (Figure 1.6) (Noel Boens, Leen, and Dehaen 2012).

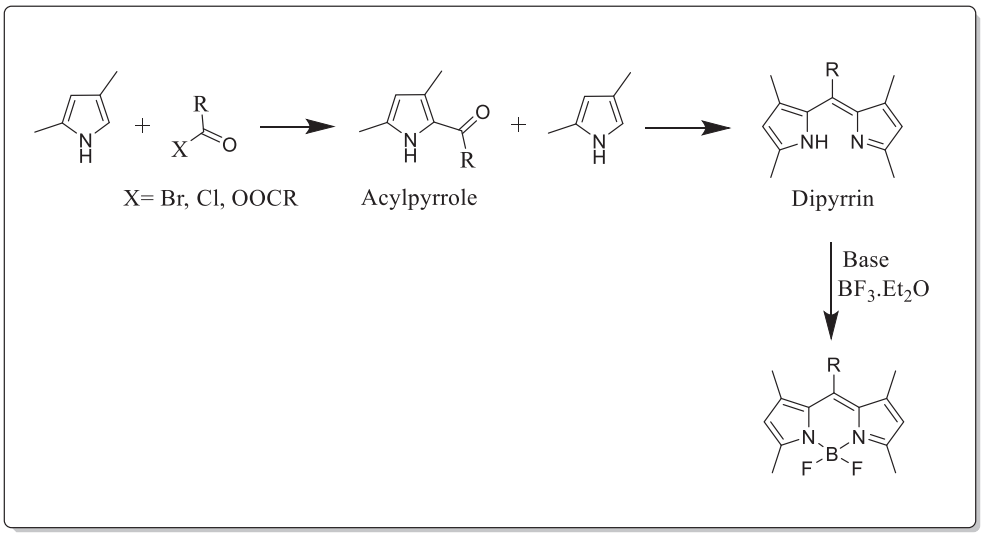

Figure 1.6. Synthesis of BODIPY dyes with the acylation of pyrrole followed by condensation and complexation
(Source: Noel Boens, Leen, and Dehaen 2012)

Before 1987, dipyrrins and oligopyrrolic molecules were known by various names, including 4,6-dipyrrin, dipyrromethene, and diaza-s-indacene. That year, guidelines for the nomenclature of such molecules were published by the IUPAC; the numbering of the BODIPY core appears in Figure 1.3, in which the central atom of the core is the *meso*-carbon, C-3 and C-5 are α-carbons, and all others are β-carbons (Figure 1.7) (Noël Boens, Verbelen, and Dehaen 2015).

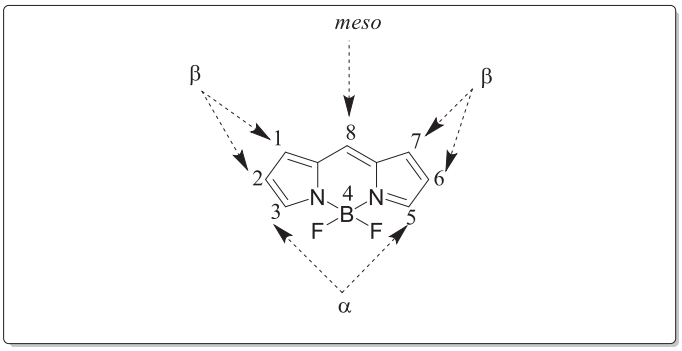

Figure 1.7. The numbering system of BODIPY core
(Source: Noël Boens, Verbelen, and Dehaen 2015)

The BODIPY core has many reactive sites that are easily functionalised with appropriate reaction mechanisms-for instance, electrophilic substitution reactions (S_EAr), Knoevenagel condensation reactions, or nucleophilic aromatic substitution reactions (S_NAr). Reactive sites of the core appear in Figure 1.8 (Noël Boens, Verbelen, and Dehaen 2015).

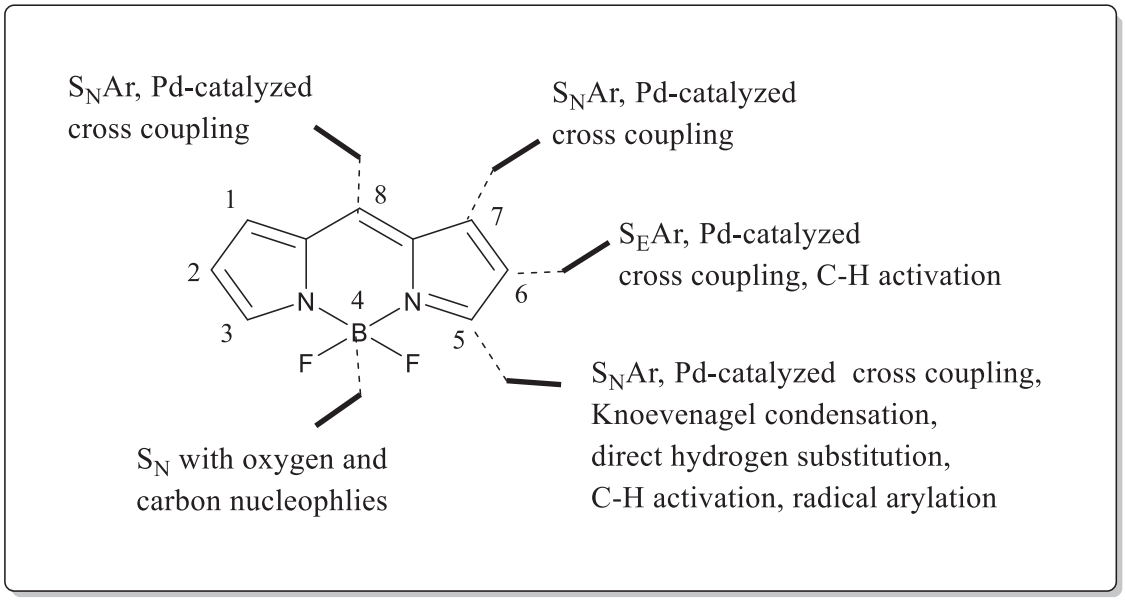

Figure 1.8. Reaction sites of BODIPY for pre- and post- modifications (Source: Noël Boens, Verbelen, and Dehaen 2015)

The BODIPY core absorbs and emits at 500-515 nm, which can easily be changed by pre- or post- alterations on the abovementioned reactive sites. For example, the BODIPY core without any substituent shows absorption and emission wavelengths and fluorescence quantum yields (φ_f=0.90) similar to those of the methylated motif on 1,3,5, and 7 carbons (φ_f=0.80) (Schmitt et al. 2009) (Wu and Burgess 2008). The introduction of halogens to the meso-position substantially decreases the fluorescence quantum yield due to the heavy atom effect, and the molecule shows non-fluorescent property (Leen et al. 2012). A similar decrease in fluorescence quantum yield is observed when the phenyl group is integrated into the BODIPY core from the same position due to the free rotation of the phenyl group (φ_f=0.03) (Yu et al. 2011). Adding methyl groups to the positions 1,3,5, and 7 counteracts the rotation of the phenyl group

and thus regenerates the fluorescence quantum yield (φ_f=0.48) (Figure 1.9) (Gabe et al. 2004).

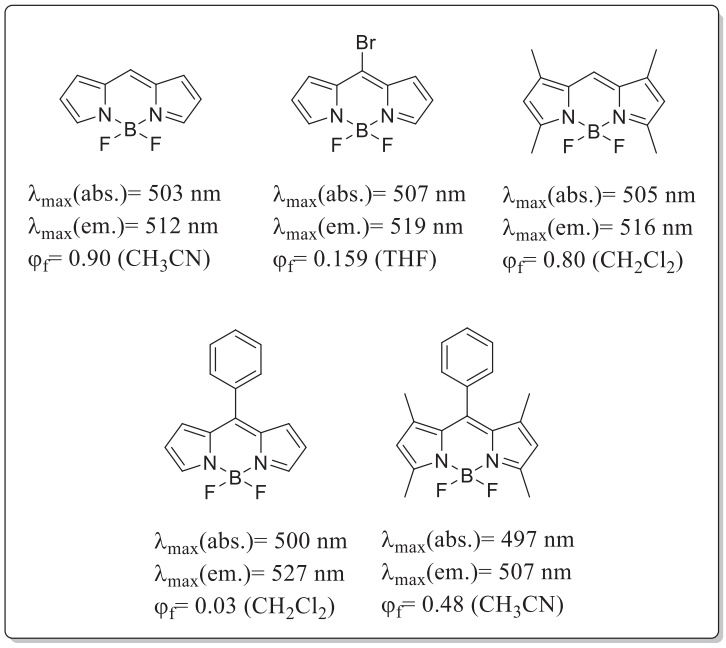

Figure 1.9. Influence of alkyl, meso halogen and aryl substituents on the spectroscopic properties

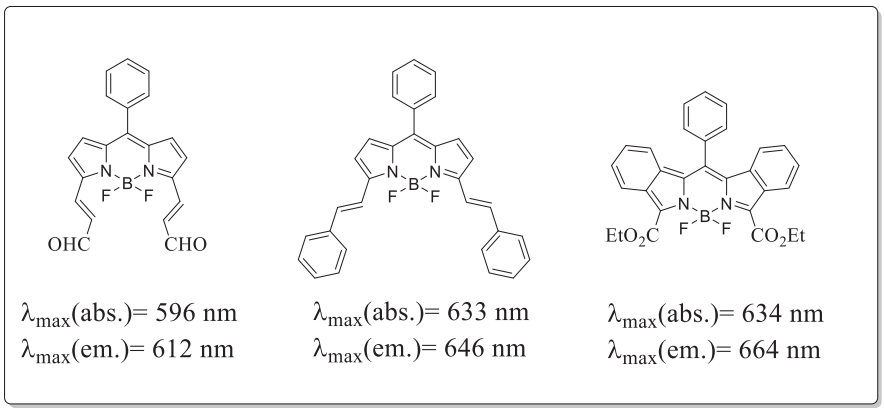

Figure 1.10. BODIPY structures with extended conjugation

Absorption and emission wavelengths can be red shifted by increasing the conjugation of dyes, either by adding unsaturated bonds, aryl groups, and aryl-attached double or triple bonds at the 3,5-positions of the BODIPY core, or by using aryl-fused or attached pyrroles as starting reagents (Figure 1.10).

In the development of fluorescent probes, BODIPY dyes have played a pivotal role relative to other dyes (e.g. rhodamine and fluorescein) because they are highly conjugated heterocyclic molecules and thus, show strong absorption in the UV-VIS region and provide high quantum yield in fluorescence emissions. The benefits of BODIPY dyes relate not only to their facile synthetic routes but also to their stability in a wide range of pH levels, temperatures, and photochemical conditions due to their high symmetrical and conjugate nature. Furthermore, they are excellent molecules for biological applications. Thanks to their ease of modification made according to the purpose of use, BODIPY dyes have wide applicability, including in photodynamic therapy (Dartar et al. 2021), dye-sensitised solar cells (Klfout et al. 2017), and the detection of metal ions (Üçüncü, Karakuş, and Emrullahoğlu 2016), reactive oxygen species (Emrullahoğlu, Üçüncü, and Karakuş 2013) and toxic gases (Sayar et al. 2018).

CHAPTER 2

LITERATURE WORKS

There are two different sensing mechanisms of gold-ions; reaction-based and coordination-based probes. In the reaction-based probes, gold ions generally activate the reactive unit (alkyne group, C = N group, etc.) of the fluorophore and trigger a series of reorganization reactions. In the coordination-based probes, gold ions make noncovalent interactions with the receptor unit.

2.1. Reaction-Based Probes

2.1.1 Cyclization Through the Alkynyl Activization

Oxygen, nitrogen, and sulfur elements are good nucleophiles thanks to their lone pair electrons. Therefore, they can easily attack the gold-activated alkyne groups then form a ring via intramolecular cyclization reaction. Based on the ring-opening principle of rhodamine dyes, three different research groups concurrently published fluorescent probes for detection of gold ions. In 2009, the first off-on type fluorescent and colorimetric probe was published (Jung Jou et al. 2009).

Propargylamine was attached to rhodamine-B as alkyne moiety. In the presence of Au^{3+} ions, spirolactam ring-opening took place and it was followed by an intramolecular cyclization reaction through the transformation of propargylamide group to oxazolecarbaldehyde without the usage of any oxidant. The probe showed highly selective recognition towards Au^{3+} ions over other metals and colorless to pink colorimetric change in EtOH/HEPES (1/1 (v/v), pH=7.4). The color and the

fluorescence changes were easily detected by the naked eye. The limit of detection was estimated as 63 ppb (Figure 2.1).

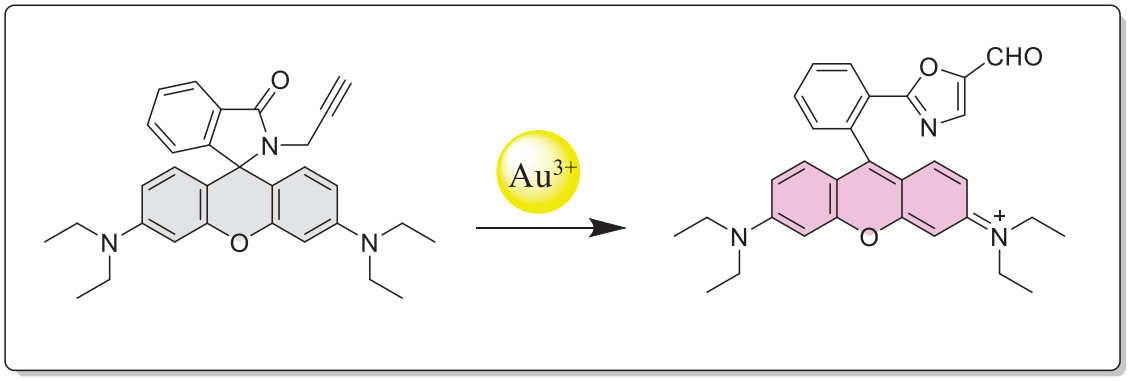

Figure 2.1 Au^{3+}-induced transformation from propargylamide to oxazolecarbaldehyde (Source:Jung Jou et al. 2009)

The fluorescence properties of the same skeleton were evaluated by Egorova's group in different media than the Jou's group. In Egorova's work the change of media to CH_3CN/PBS buffer (1/1 (v/v), pH=7.2) results in red fluorescence emission to both Au^{+} and Au^{3+} ions for the first time. The limit of detection was estimated as 0.4 ppm. Jou's and Egorova's works evinced the effect of the solvent of where the reaction took place (Figure 2.2, Figure 2.3)(Egorova et al. 2010).

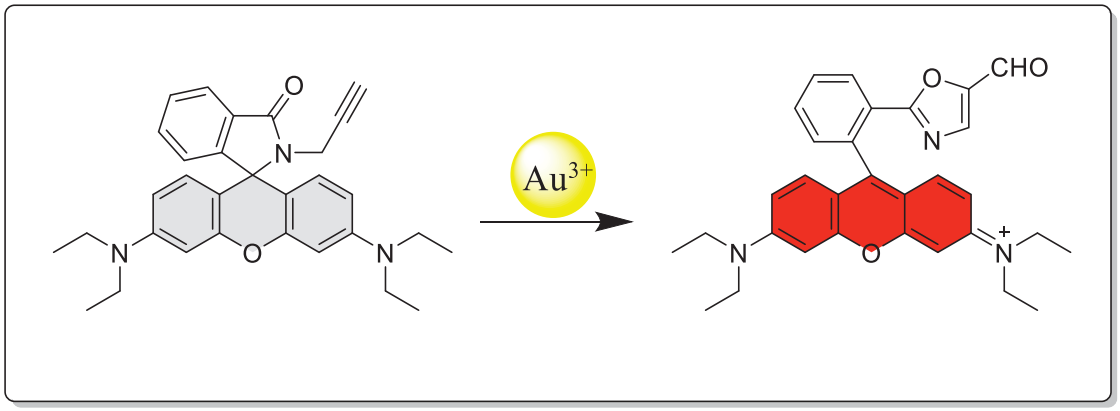

Figure 2.2. Au(I)/Au(III)-promoted sensing process (Source: Egorova et al. 2010)

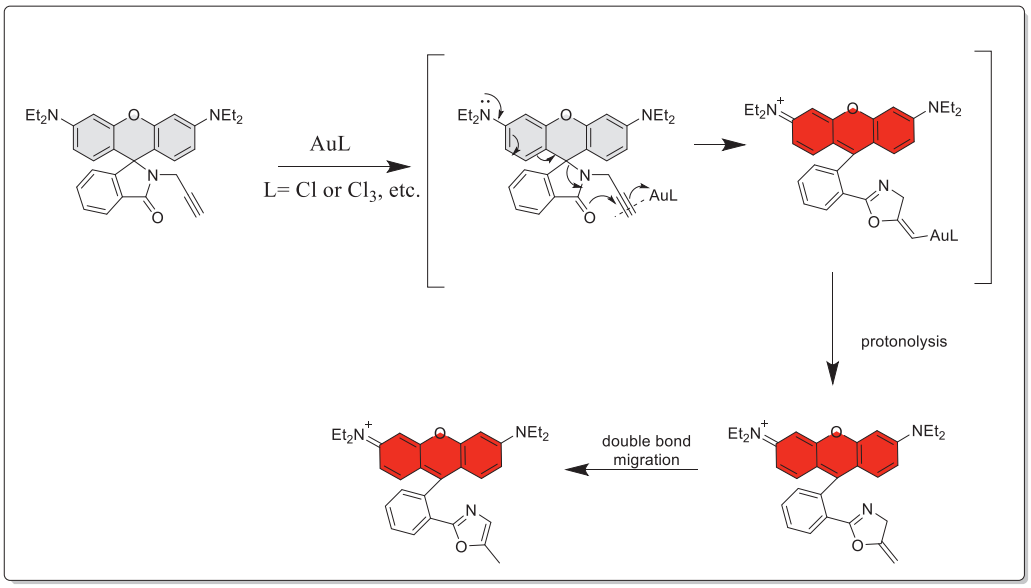

Figure 2.3. Au^{+}/Au^{3+} Promoted spirolactam ring opening of Egorova's probe (Source: Egorova et al. 2010)

Yang and his colleagues synthesized a fluorescent probe that has an irreversible reaction-based sensing mechanism which was triggered by using the alkynophilic affinity of gold ions. The non-fluorescent rhodamine hydroxamic acid dye was functionalized with an alkyne group to mediate ring-opening of the spirocyclic moiety in the presence of the Au^{3+} ions. The probe displayed highly selective and sensitive red fluorescence emission toward Au^{3+} ions in aqueous media (PBS Buffer, 1%MeOH). In aqueous media, approximately 50 nM Au^{3+} ions was detected by the probe. Besides, fluorescent imaging studies on the HeLa cell lines were demonstrated which was a promise for further biological applications (Figure 2.4) (Yang, Lee, and Tae 2009).

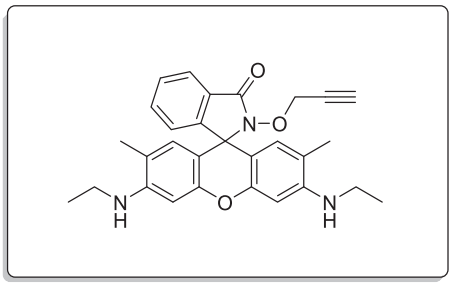

Figure 2.4. Reaction-based fluorescent sensing probe

(Source: Yang, Lee, and Tae 2009)

Our research group reported our first gold ion sensor in 2013. Alkyne unit beared rhodamine-B derivative was synthesized from 2-alknylbenzaldehyde which was the recognition site. The probe gives remarkable emission at 580 nm in CH_3CN/HEPES buffer (1/1 (v/v)) at pH=7.0 toward Au^{3+} ions and negligible emission intensity to Au^{+} ions. After the addition of Au^{3+} ions, the colorless and nonfluorescent solution turned its color to pink and showed red fluorescence emission. In order to determine the reaction mechanism of the probe, rhodamine-B was functionalized with benzaldehyde. Control molecule showed no color and fluorescence change under the same sensing conditions. The reversibility of the probe was checked with the addition of CN^{-} ions. No change was observed in colored and fluorescent solution, which was showed that the sensing process was irreversible. Additionally, the probe displayed good cell permeability and bright fluorescence signal (Figure 2.5) (Emrullahoğlu, Karakuş, and Üçüncü 2013).

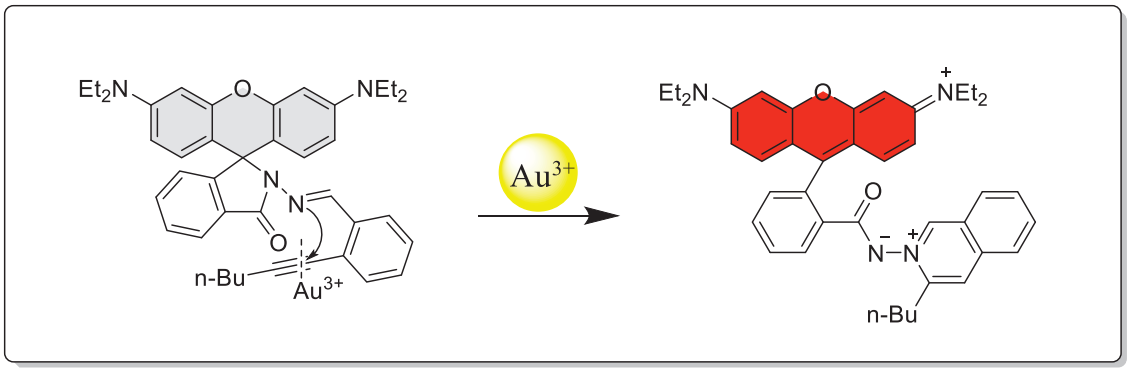

Figure 2.5. Proposed reaction mechanism of Au(III) sensing process
(Source: Emrullahoğlu, Karakuş, and Üçüncü 2013)

In 2015, our research group reported a fluorescent probe that displays a ratiometric fluorescence response towards gold and mercury ions, therefore, it is said to have dual character. Integration of BODIPY dye with the enynone moiety caused the extension of conjugation in the system, thus the probe showed fluorescence at long emission wavelength. In the recognition process, the activated alkynyl bond gave a cyclization reaction with the oxygen of the carbonyl group then produced a furan ring.

The formation of rotatable C-C bond caused a decrease in the conjugation which resulted in the shifting of emission wavelength from 562 (orange) nm to 516 nm (green). A549 lung adenocarcinoma cell lines was used in the bioimaging applications of the developed probe (Figure 2.6)(Üçüncü, Karakuş, and Emrullahoglu 2015b).

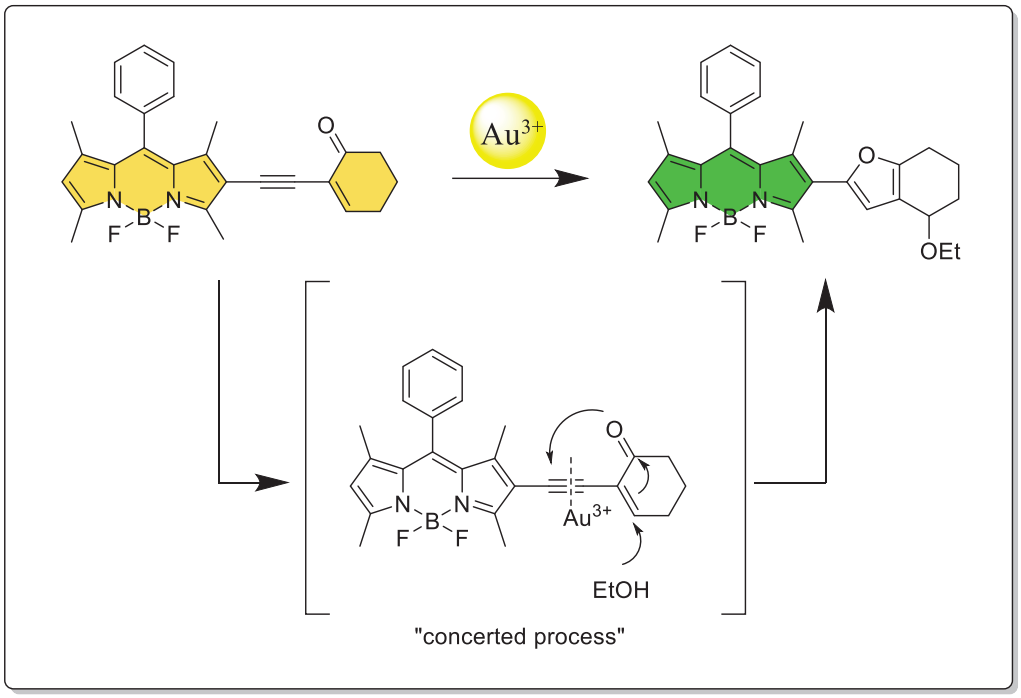

Figure 2.6. Gold-mediated cyclization
(Source: Üçüncü, Karakuş, and Emrullahoglu 2015)

Soon afterward, our group published a ratiometric BODIPY based probe comprising Z-enynol as a recognition unit. The substitution of Z-enynol generated a highly conjugated BODIPY derivative than its unsubstituted form. The probe showed fast responses to Au^{3+} ions with a distinct fluorescence change from red to green. Activation of the alkynyl bond via Au^{3+} ions triggered the cyclization reaction which disrupts the π-conjugation between the BODIPY core and enynol moiety. In the end, a highly green emissive furan derivative was formed. As the last work of the study, A549 human lung adenocarcinoma cells were cultured to record fluorescence images in the presence of Au^{3+} ions (Figure 2.7) (Üçüncü, Karakuş, and Emrullahoğlu 2016).

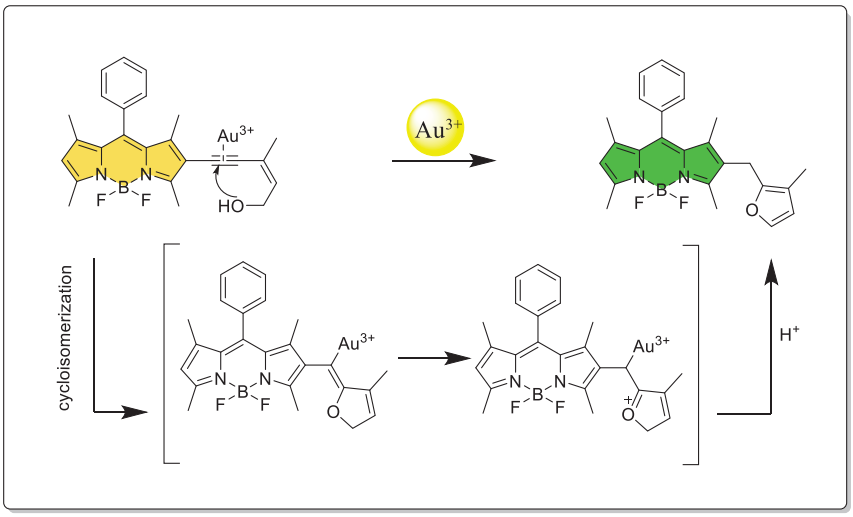

Figure 2.7. Proposed mechanism for gold ion catalyzed intramolecular cyclisation (Source: Üçüncü, Karakuş, and Emrullahoğlu 2016)

Wang and coworkers designed and synthesized a probe which undergoes Au^{3+}-promoted intramolecular hydroamination reaction in EtOH/PBS buffer (1:1, v/v, pH=7.4). The probe was non-fluorescent due to photoinduced electron transfer from aniline moiety to the BODIPY fluorophore unit. As a result of intramolecular hydroamination reaction, electron transfer is prevented and the molecule emits fluorescence at 511 nm (λ_{ex} =480 nm). The probe was also used for fluorescent imaging in HeLa cells (Figure 2.8) (J. Wang et al. 2011).

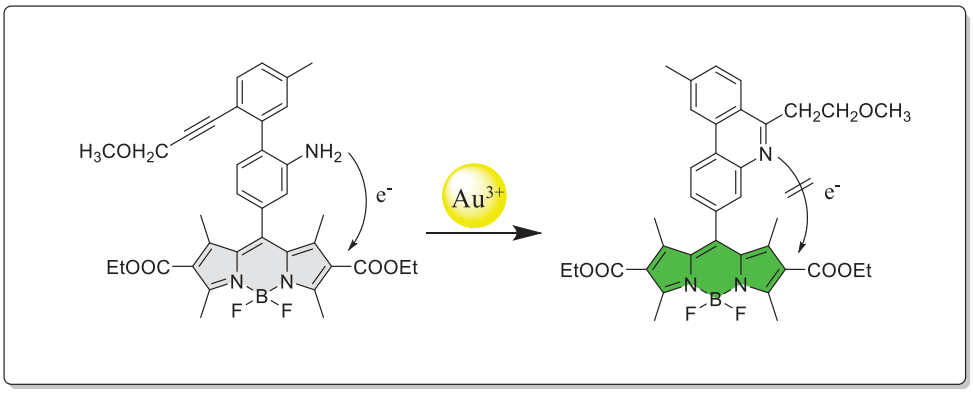

Figure 2.8. Hydroamination of probe in the presence of Au^{3+} ions (Source: J. Wang et al. 2011)

In 2016, Wang et. al was combined the 2-(phenylethynyl)aniline as reactive group with the BODIPY. Because of the electron transfer from aniline moiety to BODIPY, the probe showed no fluorescence emission. In the presence of Au^{3+} ions, the transformation of 2-(phenylethynyl)aniline to the 2-phenylindole was occurred via intramolecular cyclization reaction. This transformation blocked the PET mechanism then strong green emissive BODIPY derivative was observed. This probe detected Au^{3+} ions in real water samples and living cells (Figure 2.9) (Y. Wang et al. 2016).

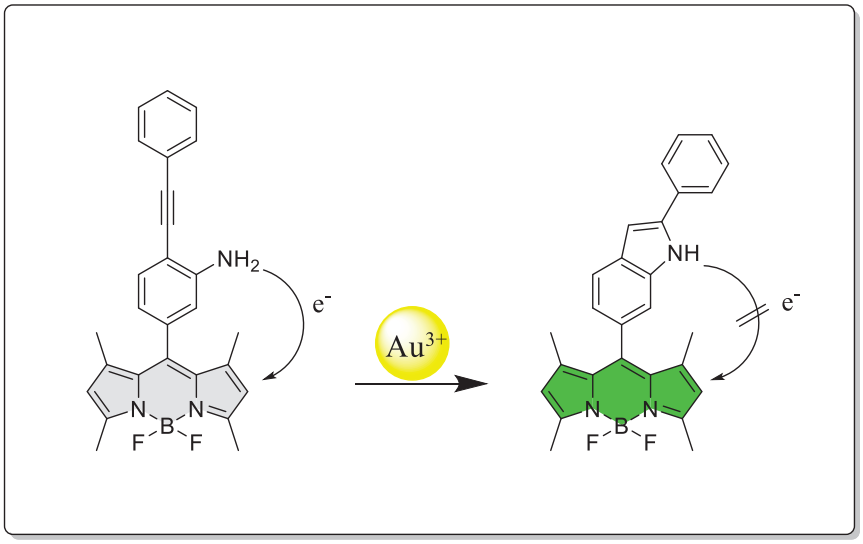

Figure 2.9. Cyclization reaction of probe in the presence of Au^{3+} ions
(Source: Y. Wang et al. 2016)

2.1.2. Cleavage of C = N Bond

For the formation of various metal complexes, imine moiety is known as an excellent ligand. The utilization of imine moiety masks the fluorescence property of fluorophore because of the non-radiative deactivation process of the excited state through isomerization of the C=N group. In 2014, our group constructed a probe by the linkage of two classical fluorophores (Rhodamine and BODIPY) by the C=N bond for the first time allowing the differential detection of Au^{3+} and Hg^{2+}. The both fluorophores were non-emissive before the addition of any metal ions because, the rhodamine part

was in the ring-closed spirolactam form and the BODIPY unit was affected by C=N isomerization. When the probe was excited to 470 nm after the addition of Au^{3+} ions, the probe showed an emission band at 506 nm which is the characteristic emission band of the BODIPY unit. On the contrary, after Au^{3+} ions were added, when the solution was excited at 525 nm, a different emission band at 585 nm was observed that refers to spirolactom ring-opening of rhodamine unit.

Treatment of the probe with Hg^{2+} ions triggered the transformation of the closed-form to the opened-form of the rhodamine unit. The emission band of rhodamine was observed at 585 nm when excited at 525 nm. However, when the solution was excited at 470 nm, no emission band was observed because the BODIPY unit was still non-emissive due to C=N moiety being conserved. The bioimaging applications of the probe were monitored in A549 lung adenocarcinoma cell lines with two reactive ions (Figure 2.10) (Karakus, Üçüncü, and Emrullahoglu 2014).

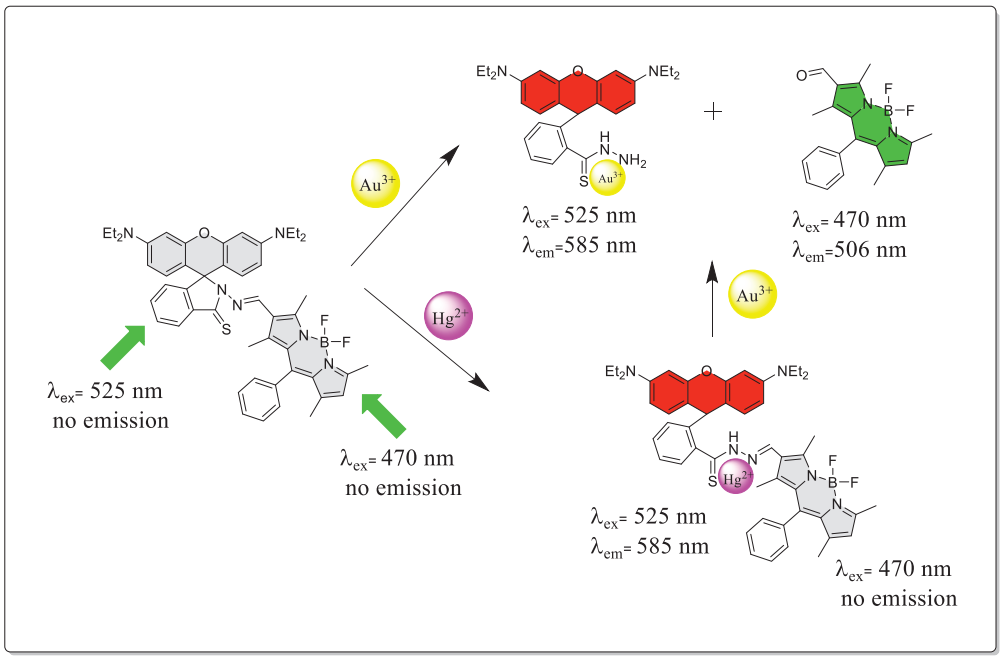

Figure 2.10. Response of probe towards the addition of Au^{3+} and Hg^{2+} ions (Source: Karakus, Üçüncü, and Emrullahoglu 2014)

Same year, a probe that includes a C=N bond was synthesized via the derivatization of BODIPY fluorophore with 2-hydrazinopyridine. Before the addition of Au^{3+} ions, the probe had no fluorescence signal for the reason mentioned above. Au^{3+} ions made coordination with both nitrogens of pyridyl and imine group then formed an intermediate. Hydrolysis of the intermediate caused the cleavage of the C=N bond thus, the emission property of BODIPY dye was recovered. The probe showed high sensitivity and selectivity to Au^{3+} ions over other metal ions. The cell imaging of the developed probe was carried out with A549 lung adenocarcinoma cell lines (Figure 2.11) (Üçüncü and Emrullahoğlu 2014).

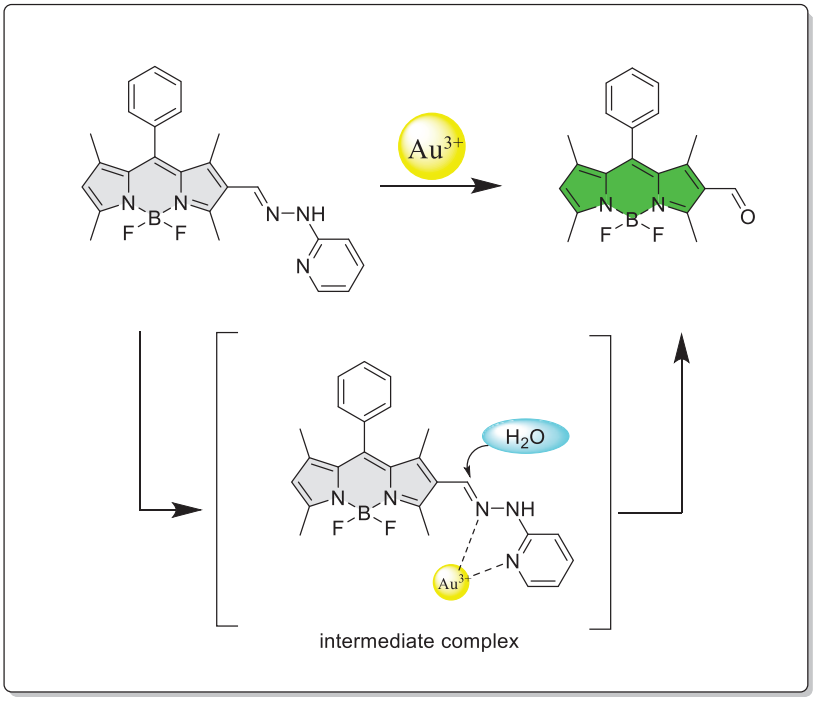

Figure 2.11. Gold mediated hydrolysis of probe
(Source: Üçüncü and Emrullahoğlu 2014)

In 2016, inspired from Emrullahoglu research groups sensor approach, two probes were constructed by embedding 2-hydrazinopyrazine and/or 2-acetylpyrazine moieties to the BODIPY core with a C=N bond as a spacer. Recognition of Au^{3+} ions by the probes was proceeded by the irreversible C=N bond hydrolysis. 2-hydrazinopyrazine derivative showed a fast response, good stability in increasing pH

and temperature compared to the 2-acetylpyrazine derivative. The bioimaging of the two probes was performed in PC12 cells. Additionally bioimaging of 2-hydrazinopyrazine derivative was examined in zebrafish. These applications were resulted in excellent cell membrane and organism permeability (Figure 2.12) (E. Wang et al. 2016).

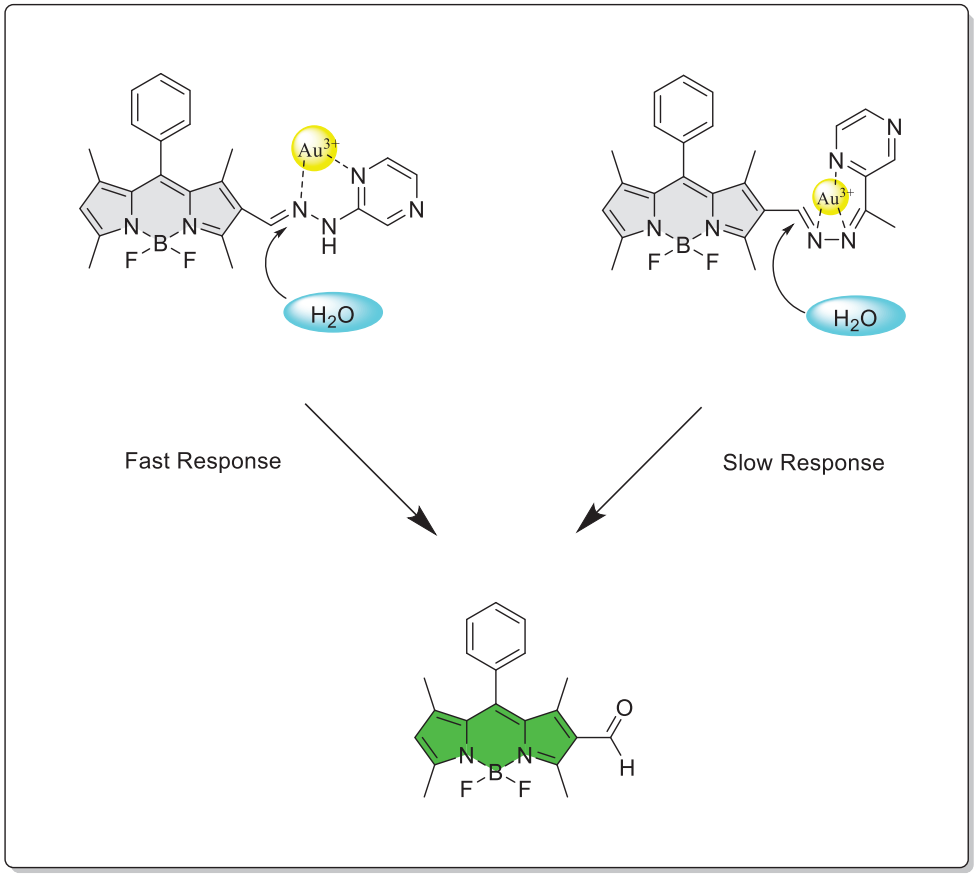

Figure 2.12. The proposed mechanism of probes with Au^{3+} ions
(Source: E. Wang et al. 2016)

2.2. Coordination Based Probes

The main challenge of designing gold ions sensors is to differentiate them from the other alkynophilic metal species such as Hg, Pd, and Ag. In order to overcome this

drawback, scientists construct probes by using the coordination of gold ions with the heteroatoms.

The first example of this strategy was reported by Wang et al. in 2011. The probe was synthesized from the condensation of rhodamine 6G hydrazide and 8-hydroxyquinoline-2-carbaldeyde followed by reduction in acetic acid with the zinc powder. The recognition was achieved by the interactions between the gold ions and heteroatoms of the probe. These interactions induced the ring-opening cyclization reaction of spirocyclic rhodamine. This probe exhibited high selectivity to Au^{3+} ions among other metal ions. To determine whether the sensing mechanism was reversible or irreversible, an excess amount of CN^- was added to the solution. As a result, the pink color of the solution evanesced and no fluorescence signal was observed; this proved that a reversible reaction took place in the sensing system. The probe was also successfully applied to HeLa cells by excellent cell membrane permeability (Figure 2.13) (J. Wang et al. 2011).

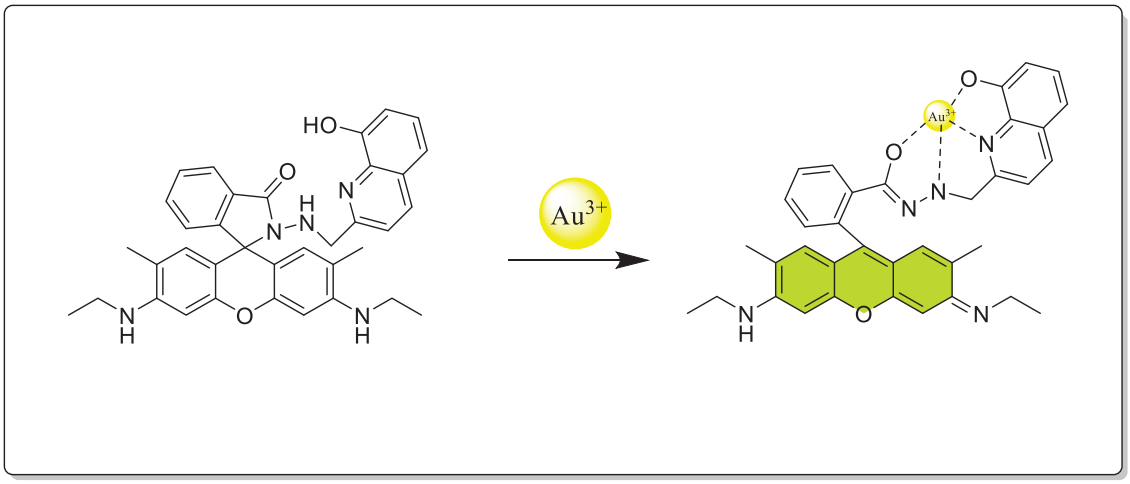

Figure 2.13. Proposed mechanism for the fluorescent changes of sensor upon the addition of Au^{3+} ions
(Source: J. Wang et al. 2011)

In more recent example reported by our research group, a probe was designed and constructed by integrating a pyridylethenyl moiety as the recognition site to a BODIPY-based fluorophore. The synthesized BODIPY derivative had faint

fluorescence emission resulting from a photoinduced intramolecular electron transfer from the pyridylethenyl unit to the BODIPY moiety. When Au^{3+} ions were added to the system, the lone pair electrons of the recognition site made a coordination with Au^{3+} ions. Therefore, the PET process could not occur hence, distinct fluorescence of the BODIPY unit was observed. The treatment of CN^- ions to the solution reduced to the fluorescence intensity of the solution, therefore, the process was considered to be reversible (Figure 2.14)(Üçüncü, Karakuş, and Emrullahoglu 2015).

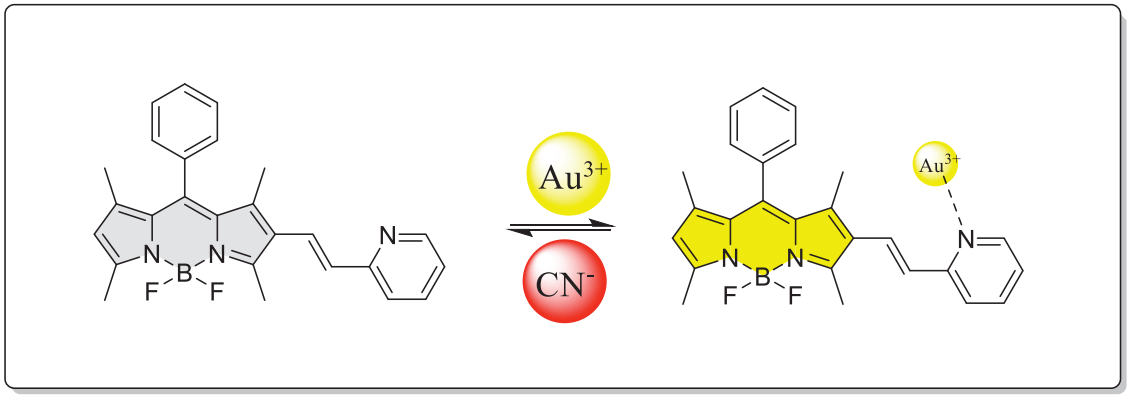

Figure 2.14. Reversible interaction of probe with Au^{3+} ions
(Source: Üçüncü, Karakuş, and Emrullahoglu 2015a)

CHAPTER 3

EXPERIMENTAL STUDY

3.1. General

All reagents were purchased from commercial suppliers (Merck) and used without any purification. ^{1}H NMR and ^{13}C NMR were measured on a Varian VNMRJ 400 Nuclear Magnetic Resonance Spectrometer and chemical shifts were calibrated using residual solvents signals ($CDCl_3$: δ (H): 7.26, δ (C): 77) or TMS. All spectroscopic measurements were performed by using DUETTA Fluorescence and Absorbance Spectrometer. Samples were contained in 10.0 mm path length quartz cuvettes (2.0 mL volume). Upon excitation at 480 nm, the emission spectra were integrated over the range of 495 nm to 750 nm. The slit width was 3 nm for both excitation and emission. The pH was measured by the HANNA HI-8014 instrument. The fluorescence images were acquired through a ZEISS Axio fluorescence microscope.

3.2. Determination of Quantum Yield

The fluorescence quantum yield of probe was determined by using an optically matching solution of Rhodamine 6G (Φ_F= 0.95 in ethanol) as a standard. The quantum yield was calculated according to the equation given below. Where Φ_F is the fluorescence quantum yield, A is the absorbance at the excitation wavelength, F is the area under the corrected emission curve, and n is the refractive index of solvents used. Subscripts S and X refer to the standard and the unknown, respectively (Figure 3.1) (Brouwer 2011).

$$\Phi_{F(x)} = \Phi_{F(s)} \times \frac{A_S}{A_x} \times \frac{F_x}{F_s} \times \frac{n_s^2}{n_x^2}$$

Figure 3.1. Formula of quantum yield
(Source: Brouwer 2011)

3.3. Determination of Detection Limit

A minimum quantity of detectable amount of analyte by an instrument or a technique is called as the detection limit and is calculated based on the fluorescence titration method. In order determine the detection limit, firstly, the emission intensity of the probe was measured ten times without metal ion to calculate the standard deviation of blank measurements. Under the optimum measurement condition, a good linear relationship between the fluorescence intensity and metal ion concentration could be obtained in the 0,1-1 equivalents. The detection limit is calculated by the following equation: detection limit = 3σbi/m, where σbi is the standard deviation of blank measurements; m is the slope of the trend line drawn by fluorescence intensity versus metal ion concentrations (Tiwari, Singh, and Sawhney 2005).

3.4 Cell Imaging

A549 Human Lung Adenocarcinoma cell lines were grown in DMEM supplemented with 10% FBS (fetal bovine serum) in an atmosphere of 5 % CO_2 at 37°C. The cells were plated on 12mm cover glasses in 6-well plate and allowed to grow for 24h. Before the experiments, the cells were washed with PBS buffer, and then the cells were incubated dye molecule (5 μM) for 20 min at 37°C then washed with PBS three times. After incubating with Au^{3+} ions (50 μM) for 20 min at 37°C, cells were rinsed with PBS three times, and DAPI for 10 min at 37°C then washed with three times. Then,

the fluorescence images were acquired through an ZEISS Axio fluorescence microscope.

3.5. Synthesis Section

The synthesis pathway for the probe molecule **BDP** consists of three parts. By using literature procedures, reactive unit, **BODIPY** based fluorophore part and the integration of them was achieved.

3.5.1. Synthesis of the Reactive Unit

Treatment of propargyl alcohol with in-situ generated $HI_{(g)}$ was procured **RU-1**. **RU-1** was coupled with phenylacetylene according to the Sonogashira coupling protocol to give **RU-2**. In the last step, alcohol group of **RU-2** was transformed to allylic bromide (**RU**) by the Appel reaction (Figure 3.2).

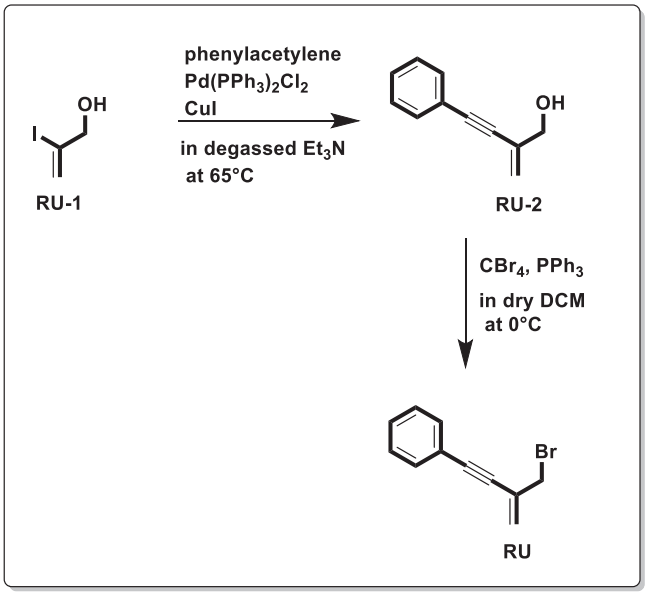

Figure 3.2. Synthesis of reactive unit

3.5.1.1 Synthesis of RU-1

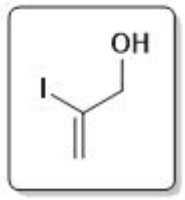

2-iodoprop-2-en-1-ol: RU-1 was synthesized according to the literature procedure (Nicolaou et al. 2006). To a stirred solution of sodium iodide (2.5 g, 16.69 mmol) in acetonitrile (22 mL) at room temperature were added TMSCl (2.12 mL, 16.69 mmol) and distilled water (0.13 mL, 8.35 mmol). After 10 minutes, propargyl alcohol (0.49 mL, 8.35 mmol) was added in one portion. After further mixing for 3 hours at room temperature, the reaction mixture was diluted with dropwise addition of distilled water (16 mL) and stirred for 30 minutes. Then, aqueous $Na_2S_2O_3$ (50 mL, 5%) was added. Mixture was extracted with diethylether (3 x 50 mL). The combined organic extracts were dried (Na_2SO_4), filtered, and concentrated under reduced pressure (at 25°C). The residue was purified by column chromatography (SiO_2, hexane/ethyl acetate 4:1) to give **RU-1** (921 mg, 60%) as a yellowish oil. ^{1}H NMR (400 MHz,$CDCl_3$) δ 6.37 (q, *J* = 1.7 Hz, 1H), 5.83 (dt, *J* = 1.9, 1.3 Hz, 1H), 4.13 (dd, *J* = 1.7, 1.2 Hz, 2H), 3.15 (s, 1H); ^{13}C NMR (101 MHz, $CDCl_3$) δ 124.49, 110.36, 70.85.

3.5.1.2 Synthesis of RU-2

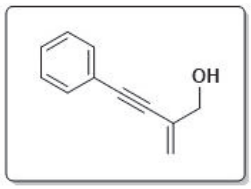

2-methylene-4-phenylbut-3-yn-1-ol: RU-2 was synthesized according to the literature procedure (Hashmi et al. 2011). **RU-1** (438 mg, 2.38 mmol) and phenylacetylene (0.31 mL, 2.86 mmol) were dissolved in degassed triethylamine (7.1 mL) under an $Ar_{(g)}$ atmosphere. To this solution $Pd(PPh)_3Cl_2$ (42.11 mg, 0.006 mmol) was added. After 10 minutes, to this solution CuI (11.42 mg, 0.006 mmol) was added. The mixture was heated at 65°C for 16 hours. After cooling to room temperature, the solvent was removed in vacuo. The crude product was purified by column chromatography (SiO_2, hexane/ethyl acetate 4:1) to afford known allyl alcohol (245 mg, 65%) as a brown oil. ^{1}H NMR (400 MHz, $CDCl_3$) δ 7.47 – 7.41 (m, 2H), 7.32 – 7.26 (m, 3H), 5.59 (q, *J* = 1.6 Hz, 1H), 5.56 (q, *J* = 1.4 Hz, 1H), 4.21 (t, *J* = 1.5 Hz, 2H), 2.32 (s, 1H); ^{13}C NMR

(101 MHz, $CDCl_3$) δ 131.67, 131.14, 128.49, 128.36, 122.76, 120.50, 90.83, 87.17, 65.15

3.5.1.3 Synthesis of RU

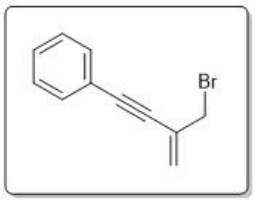

(3-(bromomethyl)but-3-en-1-yn-1-yl)benzene: By the use of Appel reaction, **RU** was synthesized (Kawato et al. 2015). Carbon tetrabromide (1.15 g, 3.46 mmol) in dry dichloromethane (2 mL) was added dropwise to a solution of RU (345 mg, 2.18 mmol) and triphenylphosphine (855.2 mg, 3.27 mmol) in dry dichloromethane at 0°C. After the addition, the cooling bath was removed and the reaction mixture was stirred at room temperature. The reaction was monitored by thin layer chromatography (TLC) until the reactant was completely consumed. Solvent was evaporated and the product was purified by column chromatography (SiO_2, hexane/ethyl acetate 10:1) to give **RU** (193 mg, 40%) as reddish oil. ^{1}H NMR (400 MHz, $CDCl_3$) δ 7.50 – 7.35 (m, 2H), 7.24 (tt, *J* = 4.3, 2.5 Hz, 3H), 5.54 (dd, *J* = 14.6, 3.9 Hz, 2H), 3.97 (d, *J* = 4.0 Hz, 2H); ^{13}C NMR (101 MHz, $CDCl_3$) δ 131.82, 131.67, 128.76, 128.45, 128.34, 124.76, 122.63, 121.31, 90.95, 87.15, 34.72.

3.5.2 Synthesis of the Fluorophore Unit

The synthesis pathway for **BDP-NH$_2$** is shown in figure 3.3. Both molecules were synthesized according to the literature procedures. **BDP-NO$_2$** was converted to its amine form using hydrazine hydrate as a reducing agent (Kusio et al. 2020), (Aydin Tekdaş et al. 2016).

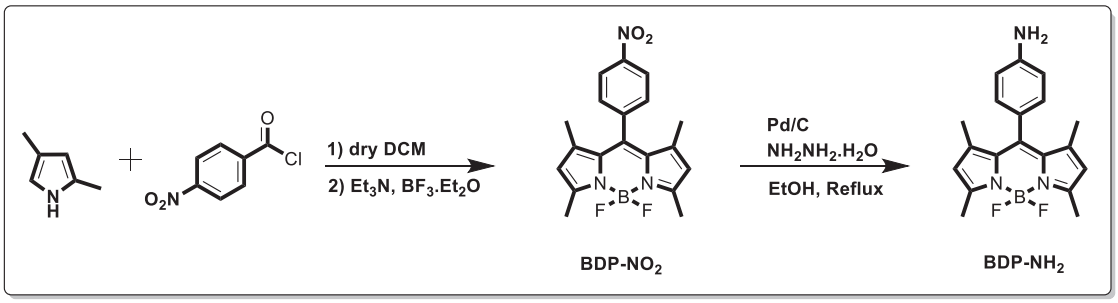

Figure 3.3. The synthesis pathway of **BDP-NH₂**

3.5.2.1. Synthesis of BDP-NO₂

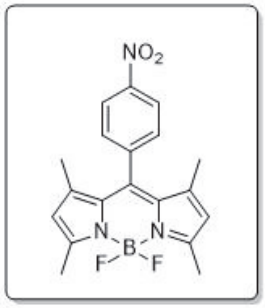

5,5-difluoro-1,3,7,9-tetramethyl-10-(4-nitrophenyl)-5H-4λ⁴,5λ⁴-dipyrrole[1,2-c:2',1'-f][1,3,2]diazaborinine: To a solution of 2,4-dimethylpyrrole (0.4 mL, 3.88 mmol) in dry dichloromethane (30 mL), 4-nitrobenzoyl chloride (326 mg, 1.76 mmol) was added under argon atmosphere and the mixture was stirred at room temperature overnight. After triethylamine (2.0 mL, 14.35 mmol) was added to the mixture, and the reaction mixture was stirred for 1 hour. Finally, boron trifluoride diethyl etherate(2.60 mL, 21.1 mmol) was added fast drop by drop and stirred at room temperature for 1 hour. The resulting solution was extracted with dichloromethane (3 x 30 mL) and dried over Na_2SO_4. The crude mixture was purified by column chromatography (SiO_2, hexane/ethyl acetate 4:1) to give **BDP-NO₂** (400 mg, 55%) as orange solid. ^{1}H NMR (400 MHz, Chloroform-d) δ 8.60 – 8.24 (m, 2H), 7.77 – 7.39 (m, 2H), 6.02 (s, 2H), 2.56 (s, 6H), 1.36 (s, 6H); ^{13}C NMR (101 MHz, $CDCl_3$) δ 156.66, 148.30, 142.51, 141.94, 138.30, 130.60, 129.63, 124.36, 123.92, 121.86, 14.7, 14.69.

3.5.2.2. Synthesis of BDP-NH_2

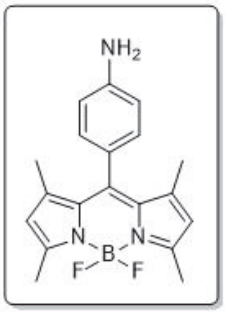

4-(5,5-difluoro-1,3,7,9-tetramethyl-5H-4λ^4,5λ^4-dipyrrolo[1,2-c:2',1'-f] [1,3,2]diazaborinin-10-yl)aniline: To a solution of BDP-NO_2 (100 mg, 0.27 mmol) was dissolved in ethanol (8 mL) under argon atmosphere were added 10% Pd/C (29 mg, 0.27 mmol) and hydrazine hydrate (0.28 mL, 5.75 mmol, 98%). The reaction mixture was heated at reflux temperature under argon atmosphere for 2 hours, then it was cooled to room temperature and filtered through the celite. The solvent was removed by rotary evaporation. The resultant residue was purified by column chromatography (SiO_2, dichloromethane) to afford **BDP-NH_2** as red solid (73 mg, 80%). ^{1}H NMR (400 MHz, Chloroform-d) δ 7.12 – 6.93 (m, 2H), 6.77 (dp, J = 6.0, 2.1 Hz, 2H), 5.96 (d, J = 4.0 Hz, 2H), 3.89 (s, 2H), 2.54 (d, J = 4.0 Hz, 6H), 1.49 (d, J = 3.9 Hz, 6H); ^{13}C NMR (101 MHz,$CDCl_3$) δ 154.91, 147.00, 143.18, 142.64, 131.99, 128.90, 124.62, 120.93, 120.90, 115.39, 14.62, 14.52.

3.5.3. Synthesis of Probe (BDP)

N-alkylation of the aniline moiety of the fluorophore unit was performed by the literature procedure (Figure 3.4) (Y. Li et al. 2014).

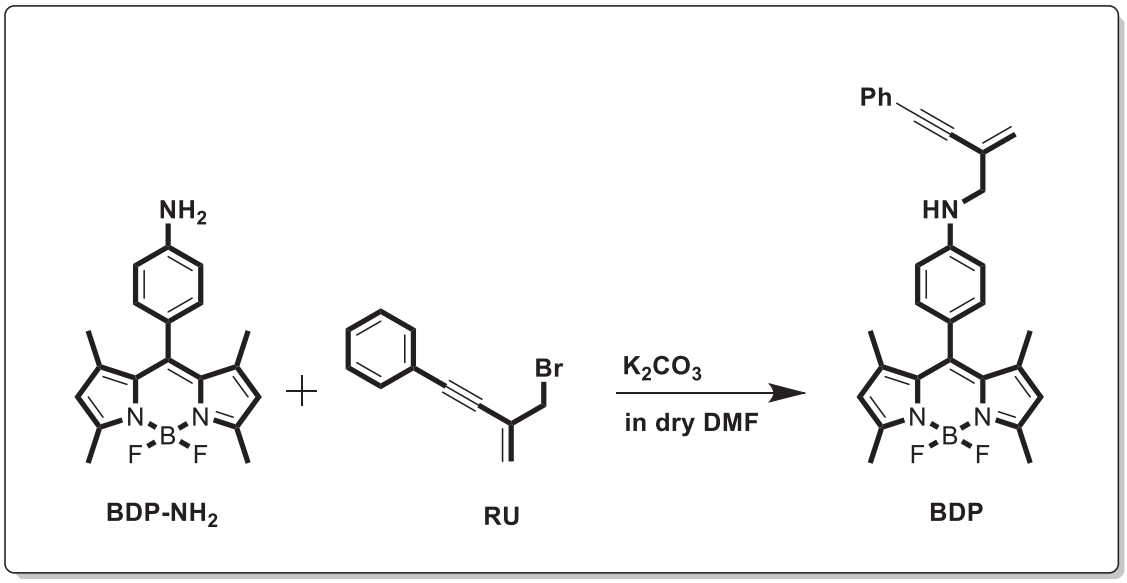

Figure 3.4. Synthesis of Probe (**BDP**)

4-(5,5-difluoro-1,3,7,9-tetramethyl-5H-4λ^4,5λ^4-dipyrrolo[1,2-c:2',1'-f][1,3,2]diazaboronin-10-yl)-N-(2-metylene-4-phenylbut-3-yn-1-yl)aniline: **BDP-NH$_2$** (150 mg, 0.44 mmol) was dissolved in dry DMF (3 mL). To this solution were added **RU** (115 mg, 0.52 mmol) and potassium carbonate (70 mg, 0.50 mmol) under the argon atmosphere. The reaction mixture was heated at 80°C for 24 hours. The mixture was extracted with ethyl acetate (3 x 50 mL). The combined organic extracts were dried (Na2SO4), filtered, and concentrated under reduced pressure. The residue was purified by column chromatography (SiO_2, hexane/ethyl acetate 10:1) to give **BDP** (21 mg, 10%) as an orange solid. ^{1}H NMR (400 MHz, Chloroform-d) δ 7.52 – 7.40 (m, 2H), 7.39 – 7.27 (m, 3H), 7.07 – 6.99 (m, 2H), 6.78 – 6.70 (m, 2H), 5.96 (s, 2H), 5.57 (dq, J = 22.2, 1.4 Hz, 2H), 4.31 (s, 1H), 3.99 (d, J = 1.5 Hz, 2H), 2.54 (s, 5H), 1.26 (s, 8H); ^{13}C NMR (101 MHz, $CDCl_3$) δ 154.86, 143.18, 142.74, 132.05, 131.61, 128.88, 128.54, 128.45, 128.35, 122.67, 120.89, 90.88, 87.64, 53.39, 31.90, 30.56, 29.68, 22.67, 14.59, 14.55, 14.53, 14.50, 14.10.

CHAPTER 4

RESULTS AND DISCUSSION

In this thesis study, a novel BODIPY-based fluorescent chemosensor (**BDP**) appended with an enyne moiety was designed, synthesized, and characterized, with the expectation of generating non-fluorescent BODIPY derivatives due to the PET-based (i.e., photo-induced electron transfer) quenching principle. Based on previous studies in our research group related to gold ion sensors, we had the knowledge about the alkynophilic property of gold ions. It is known from the literature that most molecular sensors devised for gold ions use triple bonds as recognition site. In the light of this consideration, enyne moiety which consists of a double and a triple bond was used as a recognition site. The sensitivity and selectivity of the probe was carefully investigated. Also, bioimaging application was performed successfully.

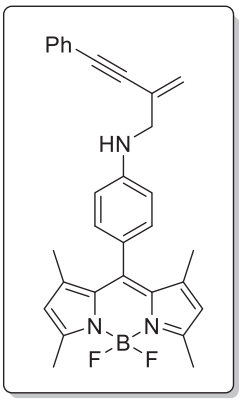

Figure 4.1. **BDP**

The spectroscopic investigations started with the evaluations of the optical behaviors of **BDP** in different reaction mediums. Considering that probe **BDP** is not

completely water soluble thus, EtOH/PBS (v/v, 1:1, pH = 7.0), EtOH/Phosphate buffer solution (v/v, 1:1, pH = 7.0), and CH_3CN/HEPES buffer solution (v/v, 1:1, pH = 7.0) mediums were examined for the response to Au^{3+} ions. The highest increment in fluorescence intensity was observed in EtOH/PBS (v/v, 1:1, pH = 7.0) solvent system for Au^{3+} ions. Moreover, the effect of the ratio of water in the EtOH/PBS medium on the spectral behaviors of **BDP** was evaluated. EtOH/PBS (v/v, 6:4, pH = 7.0) medium gave the highest fluorescence intensity when the probe excited at 480 nm. However, EtOH/PBS (v/v, 1:1, pH = 7.0) was decided as a reaction medium because of the applicability of the probe to cell imaging (Figure 4.2.a).

Then, the effect of pH was surveyed in the pH range 2-13. In the absence of Au^{3+} ions, **BDP** was quite stable, even in strongly acidic and basic mediums. A spectacular increase in fluorescence intensity was observed at pH 2-9 upon the addition of Au^{3+} ions. The detection system did not work at pH 10-13 although Au^{3+} ions were in presence. Thus, the pH of the reaction medium was chosen as 7.0 for physiological application (Figure 4.2.b).

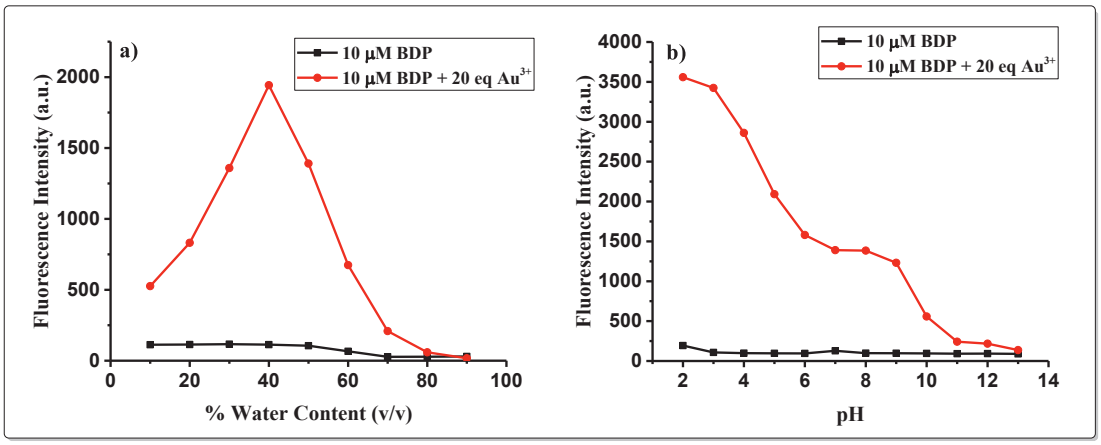

Figure 4.2. a) Effect of fraction of water on the fluorescence intensity of **BDP** (in PBS buffer pH 7.0/EtOH) black line; in absence of Au^{3+} ions, red line; in presence of Au^{3+} ions (20 eq.) (λ_{ex}: 480 nm, λ_{em}= 515 nm at 25°C), b) Effect of pH on the fluorescence intensity of **BDP** (10 µM) in EtOH/PBS (v/v, 1:1, pH = 7.0) black line; in absence of Au^{3+} ions, red line; in presence of Au^{3+} ions (20 eq.) (λ_{ex}: 480 nm, λ_{em}= 515 nm at 25°C)

UV/Vis spectrum of free **BDP** in EtOH/PBS (v/v, 1:1, pH = 7.0) showed a maximum absorption band at 498 nm, which belongs to the BODIPY core. After the addition of Au^{3+} ions, the absorption band decreased and shifted to 500 nm (Figure 4.3.a). As expected, the resultant compound was non-fluorescent due to the PET process in EtOH/PBS (v/v, 1:1, pH = 7.0). The fluorescence spectrum of **BDP** collected upon excitation at 480 nm exhibited a very weak emission band at 516 nm. However, emission intensity was 11-fold increased at 515 nm after the addition of Au^{3+} ions (200 µM, 20 equivalents with respect to probe **BDP**). The remarkable change in emission of the probe is the evidence of the blocking of the PET process (Figure 4.3.b).

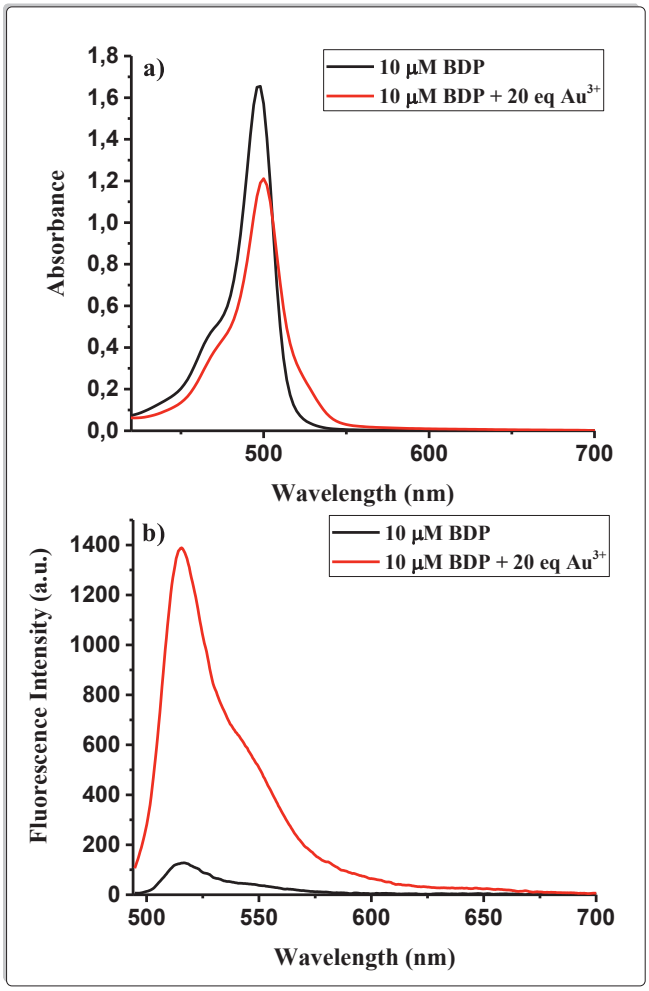

Figure 4.3. a)Absorption and b) emission spectra of **BDP** (10 µM) and Au^{3+} ions (20 eq.) in EtOH/PBS (v/v, 1:1, pH = 7.0); (λ_{ex}: 480 nm, λ_{em}= 515 nm at 25°C)

The reaction time profile of the sensing event was examined by the addition of Au^{3+} ions to the sensing media. The spectroscopic response of probe **BDP** was quite fast (< 1 min), the highest signal intensity was observed at the 4th minute. The signal intensity remained constant after 10 min, which was lower than the intensity at the 4th minute. Based on these, all measurements were carried out after 4 min, allowing the fluorescence signal to reach the maxima (Figure 4.4.a).

A systematic titration of **BPD** with Au^{3+} ions indicated that emission band intensity at 515 nm increases linearly with the increasing concentration of Au^{3+} ions in the range of 0.0–200 μM. The solution became saturated after the addition of 20 eq. Au^{3+} ions (Figure 4.4.b).

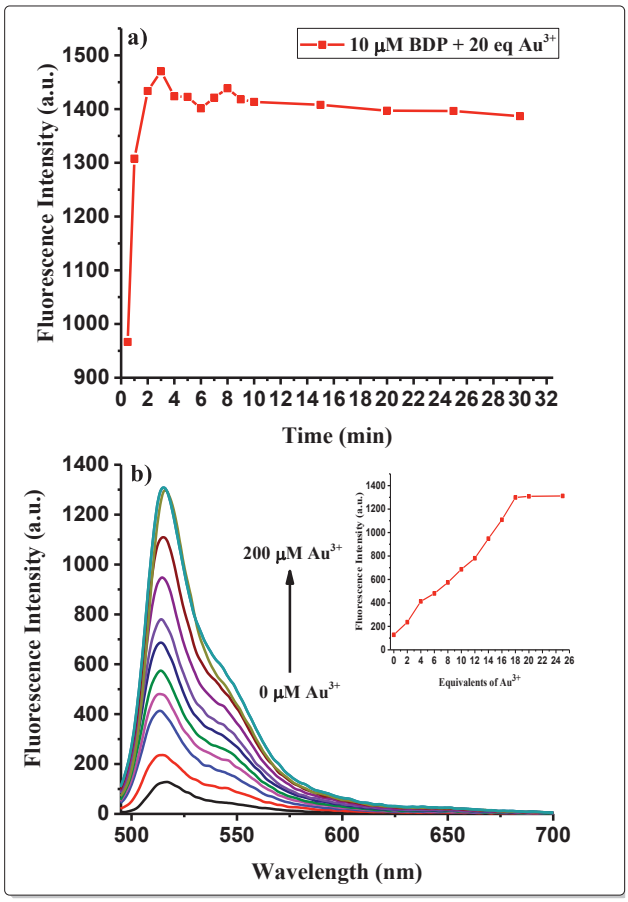

Figure 4.4. a) Time-dependent fluorescence change of **BDP** (10 μM) in the presence of an 20 equivalent of Au^{3+} ions measured in EtOH/PBS (v/v, 1:1, pH = 7.0), b) Fluorescence spectra of **BDP** (10 μM) in EtOH/PBS (v/v, 1:1, pH = 7.0) in the presence of Au^{3+} ions (mole equivalents = 0-20), Inset: Calibration curve. (λ_{ex}: 480 nm at 25 ºC).

Furthermore, the selectivity of **BDP** was determined by titrating it with various metal cations under optimum conditions. The probe was proved to be highly selective for Au^{3+} ions. The higher response of Au^{+} and Hg^{2+} ions compared to other metal ions can be explained by similar alkynophilic properties to Au^{3+} ions (Figure 4.5.a).

The interference of other metal ions in the detection of Au^{3+} ions was investigated. The results showed that **BDP** could smoothly detect the Au^{3+} ions in the presence of other metal ions (Figure 4.5.b).

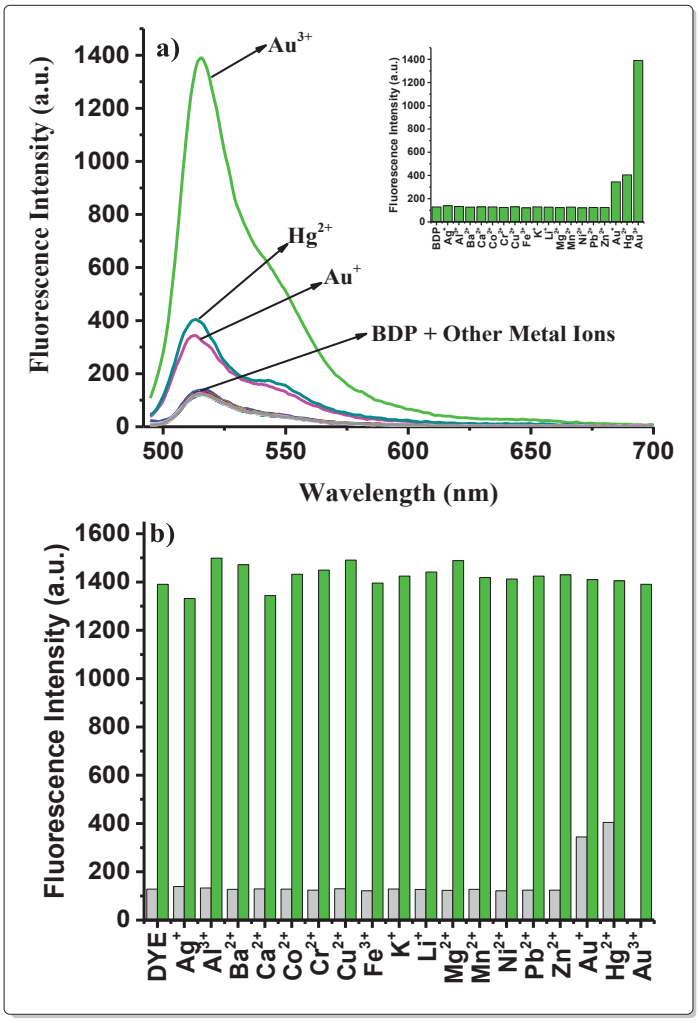

Figure 4.5. a) Fluorescence of selectivity experiment of **BDP** (10 μM) + Au^{3+} ions (200 μM, 20 eq.), **BDP** (10 μM) + other metal ions (200 μM, 20 eq.) in EtOH/PBS (v/v, 1:1, pH = 7.0) (λ_{ex}: 480 nm, at 25 ºC). Inset: Bar graph notation, b) Fluorescence of a competition experiment of **BDP** (10 μM) in EtOH/PBS (v/v, 1:1, pH = 7.0) in presence of 20 equivalents of the cations (grey bar); in presence of cations and Au^{3+} ions

Lastly, titration with lower concentrations was performed to determine the detection limit of **BDP** towards Au^{3+} ions. The increased emission intensity was directly proportional to the amount of Au^{3+} ions and the minimum amount of Au^{3+} ions that can be detected under optimum conditions was found to be 10 nM based on S/N = 3 (R^2 = 0.994) (Figure 4.6).

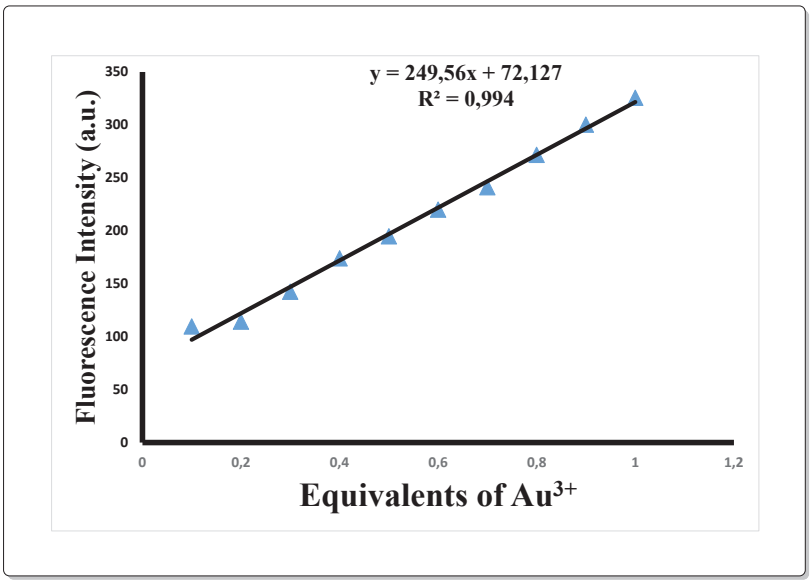

Figure 4.6. Fluorescence changes of **BDP** (10 μM) upon addition of Au^{3+} ions (0.1 to 1.0 eq.) in EtOH/PBS (v/v, 1:1, pH = 7.0), (λ_{ex}: 480 nm, at 25 °C)

Intramolecular hydroamination reaction took place with the treatment of **BDP** with a catalytic amount of Au^{3+} ions in ethanol and resulted in the appearance of a strong green-fluorescent solution which is **BDP-PYR** including 2,4-disubstituted pyrrole (Figure 4.7). Two major products with close Rf values were monitored by TLC and separated by column chromatography. However, structural information of purified products could not be determined by ^{1}H NMR, instead, cyclization product was characterized by HRMS.

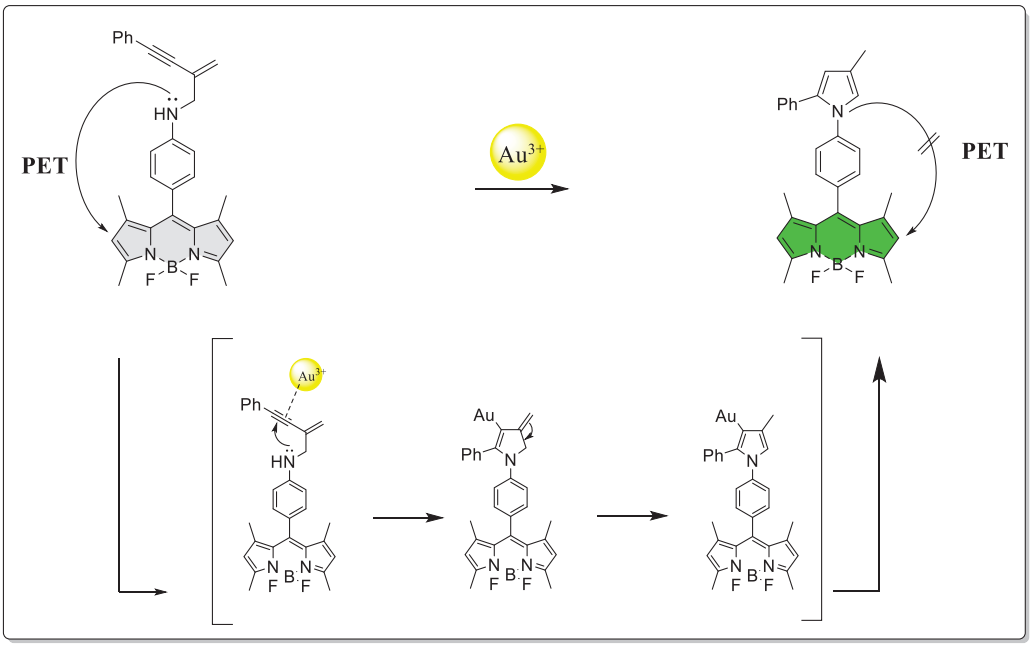

Figure 4.7. Proposed reaction mechanism for the detection of Au^{3+} ions

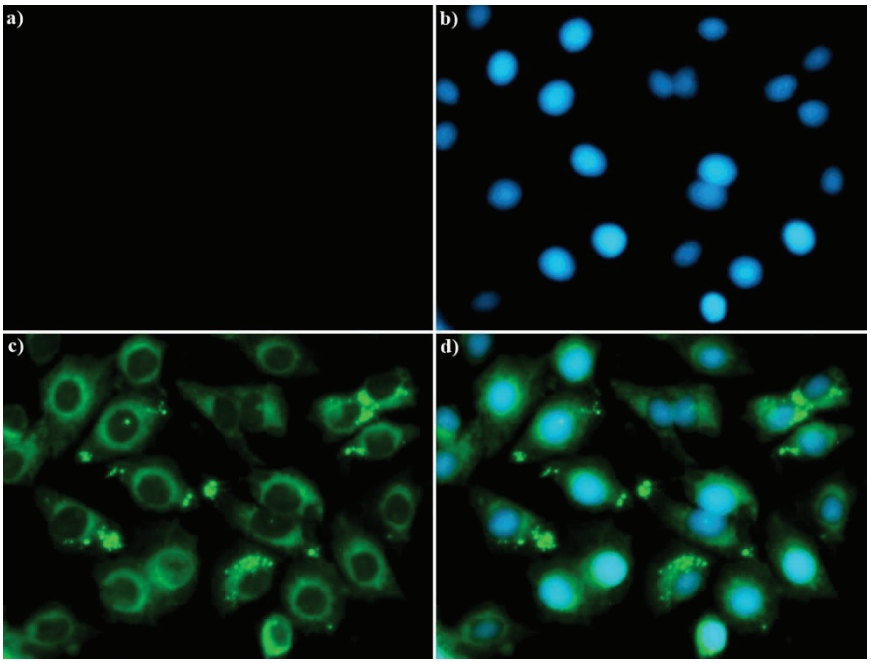

Figure 4.8.Fluorescence images of Human Lung Adenocarcinoma cells (A549). a)Fluorescence image of A549 cells treated with **BDP** (5 μM) only; b) Fluorescence image of cells treated with DAPI (control); c) Fluorescence image of cells treated with **BDP** (5 μM) and Au^{3+} ions (50 μM) (λ_{ex} = 480 nm); d) merged images of frames b-c.

Finally, the applicability of probe **BDP** for imaging Au^{3+} ions in living milieu was questioned relying on the extreme photochemical and physical properties of probe **BDP,** including its rapid response time, unique gold ion specificity, low detection limit, and high fold fluorescent change. To this end, firstly, Human Lung Adenocarcinoma cells (A549) were incubated with probe (5 μM) at 37°C for 20 min. Then, 50 μM Au^{3+} solution was added and the cells were incubated for 20 min. Finally, the cells were also incubated for another 10 min after the addition of DAPI staining dye which stains the nucleus of the cell. Fluorescence images of the probe were taken in the absence and presence of Au^{3+} ions in the cell medium (Figure 4.8).

CHAPTER 5

CONCLUSION

In this research, a novel "turn-on" fluorescent chemosensor was designed, synthesized, characterized towards the detection of Au^{3+} ions, and its sensing capacity to other possible reactive species was examined. The probe was designed based on the alkynophilic property of Au^{3+} ions. Therefore, enyne which includes the C-C triple bond was combined with a fluorophore unit which was chosen as BODIPY. Resulting chemosensor had non-fluorescent property because of the PET process. The addition of Au^{3+} ions activated alkyne moiety and induced intramolecular hydroamination reaction. Therefore, the PET process was blocked, and strong green-fluorescent emission was observed.

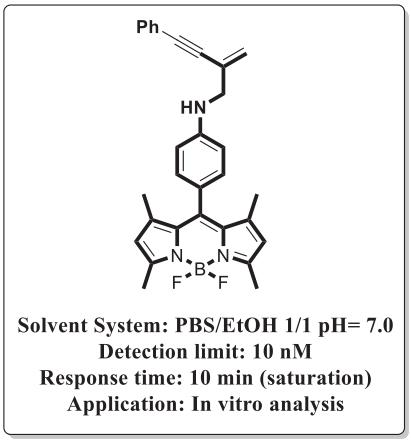

Figure 5.1. Properties of **BDP**

The photophysical properties of the probe, **BDP**, were systematically scrutinized by the aid of UV/Vis and Fluorescence spectrophotometry. **BDP** has no fluorescent emission (Φ_F=0.0049) upon excitation at 480 nm. The probe showed distinct fluorescent

response(Φ_F=0.49) and extremely low detection limit (10 nM) toward Au^{3+} ions. The probe selectively and sensitively detected Au^{3+} ions without any interference of competitive metal ions.

Apart from the rapid and specific response to Au^{3+} ions in the solution, this probe proved to be highly successful in imaging gold species in human lung adenocarcinoma (A549) cells.

REFERENCES

Aydin Tekdaş, Duygu, Geetha Viswanathan, Sevinc Zehra Topal, Chung Yeng Looi, Won Fen Wong, Grace Min Yi Tan, Yunus Zorlu, Ayşe Gül Gürek, Hong Boon Lee, and Fabienne Dumoulin. 2016. "Antimicrobial Activity of a Quaternized BODIPY against Staphylococcus Strains." Organic and Biomolecular Chemistry 14 (9): 2665–70 https://doi.org/10.1039/c5ob02477c.

Boens, Noel, Volker Leen, and Wim Dehaen. 2012. "Fluorescent Indicators Based on BODIPY." Chemical Society Reviews 41 (3): 1130–72. https://doi.org/10.1039/c1cs15132k.

Boens, Noël, Bram Verbelen, and Wim Dehaen. 2015. "Postfunctionalization of the BODIPY Core: Synthesis and Spectroscopy." European Journal of Organic Chemistry 2015 (30): 6577–95. https://doi.org/10.1002/ejoc.201500682.

Boyer, Josepih H, Anthony M Haag, Govindarao Sathyamoorthi, and Theodore G Pavlopoulos. 1993. "Pyrromethene-BF2, Complexes as Laser Dyes: 2." Heteroat. Chem. 4 (1): 39–49.

Brouwer, Albert M. 2011. "Standards for Photoluminescence Quantum Yield Measurements in Solution (IUPAC Technical Report)." Pure and Applied Chemistry 83 (12): 2213–28. https://doi.org/10.1351/PAC-REP-10-09-31.

Carter, Kyle P, Alexandra M Young, and Amy E Palmer. 2014. "Fluorescent Sensors for Measuring Metal Ions in Living Systems." Chemical Reviews. https://doi.org/10.1021/cr400546e.

Cheng, Jinghui, Xiangge Zhou, and Haifeng Xiang. 2015. Fluorescent Metal Ion Chemosensors via Cation Exchange Reactions of Complexes, Quantum Dots, and Metal-Organic Frameworks. Analyst. Vol. 140. Royal Society of Chemistry. https://doi.org/10.1039/c5an01398d.

Dartar, Suay, Muhammed Ucuncu, Erman Karakus, Yuqi Hou, Jianzhang Zhao, and Mustafa Emrullahoglu. 2021. “BODIPY-Vinyl Dibromides as Triplet Sensitisers for Photodynamic Therapy and Triplet-Triplet Annihilation Upconversion.” Chemical Communications 57 (49): 6039–42. https://doi.org/10.1039/d1cc01881g.

Das, Sudipta, Mili Dutta, and Debasis Das. 2013. “Fluorescent Probes for Selective Determination of Trace Level Al 3+: Recent Developments and Future Prospects.” Analytical Methods 5 (22): 6262–85. https://doi.org/10.1039/c3ay40982a.

Duke, Rebecca M., Emma B. Veale, Frederick M. Pfeffer, Paul E. Kruger, and Thorfinnur Gunnlaugsson. 2010. “Colorimetric and Fluorescent Anion Sensors: An Overview of Recent Developments in the Use of 1,8-Naphthalimide-Based Chemosensors.” Chemical Society Reviews 39 (10): 3936–53. https://doi.org/10.1039/b910560n.

Egorova, Olga A., Hyewon Seo, Amrita Chatterjee, and Kyo Han Ahn. 2010. “Reaction-Based Fluorescent Sensing of Au(I)/Au(III) Species: Mechanistic Implications on Vinylgold Intermediates.” Organic Letters 12 (3): 401–3. https://doi.org/10.1021/ol902395x.

Emrullahoğlu, Mustafa, Erman Karakuş, and Muhammed Üçüncü. 2013. “A Rhodamine Based ‘Turn-on’ Chemodosimeter for Monitoring Gold Ions in Synthetic Samples and Living Cells.” Analyst 138 (13): 3638–41. https://doi.org/10.1039/c3an00024a.

Emrullahoğlu, Mustafa, Muhammed Üçüncü, and Erman Karakuş. 2013. “A BODIPY Aldoxime-Based Chemodosimeter for Highly Selective and Rapid Detection of Hypochlorous Acid.” Chemical Communications 49 (71): 7836–38. https://doi.org/10.1039/c3cc44463e.

Gabe, Yu, Yasuteru Urano, Kazuya Kikuchi, Hirotatsu Kojima, and Tetsuo Nagano. 2004. “Highly Sensitive Fluorescence Probes for Nitric Oxide Based on Boron Dipyrromethene Chromophore - Rational Design of Potentially Useful

Bioimaging Fluorescence Probe." Journal of the American Chemical Society 126 (10): 3357–67. https://doi.org/10.1021/ja037944j.

Hashmi, A. Stephen K., Matthias Rudolph, and Frank Rominger. 2011. "Cyclization of 2-Alkynylallyl Alcohols to Highly Substituted Furans by Gold(I)-Carbene Complexes." European Journal of Organic Chemistry, no. 4: 667–71. https://doi.org/10.1002/ejoc.201001479.

Hashmi, A Stephen K, and Matthias Rudolph. 2008. "Gold Catalysis in Total Synthesis." Chemical Society Reviews 37 (9): 1766–75. https://doi.org/10.1039/b615629k.

Jung Jou, Min, Xiaoqiang Chen, K. M.K. Swamy, Ha Na Kim, Hae Jo Kim, Sang Gi Lee, and Juyoung Yoon. 2009. "Highly Selective Fluorescent Probe for Au3+ Based on Cyclization of Propargylamide." Chemical Communications, no. 46: 7218–20. https://doi.org/10.1039/b917832e.

Karakuş, Erman, Gulcin Cakan-Akdogan, and Mustafa Emrullahoglu. 2015. "A Guanidinium Modified Rhodamine-Based Fluorescent Probe for in Vitro/Vivo Imaging of Gold Ions." Analytical Methods 7 (19): 8004–8. https://doi.org/10.1039/c5ay01581b.

Karakus, Erman, Muhammed Üçüncü, and Mustafa Emrullahoglu. 2014. "A Rhodamine/BODIPY-Based Fluorescent Probe for the Differential Detection of Hg(Ii) and Au(Iii)." Chemical Communications 50 (9): 1119–21. https://doi.org/10.1039/c3cc48436j.

Kawato, Yuji, Akino Kubota, Hiromi Ono, Hiromichi Egami, and Yoshitaka Hamashima. 2015. "Enantioselective Bromocyclization of Allylic Amides Catalyzed by BINAP Derivatives," 17–20. https://doi.org/10.1021/acs.orglett.5b00220.

Klfout, Hafsah, Adam Stewart, Mahmoud Elkhalifa, and Hongshan He. 2017. "BODIPYs for Dye-Sensitized Solar Cells." ACS Applied Materials and Interfaces 9 (46): 39873–89. https://doi.org/10.1021/acsami.7b07688.

Knosp, Helmut, Richard J Holliday, and Christopher W Corti. 2003. “Gold in Dentistry: Alloys, Uses and Performance.” Gold Bulletin 36 (3): 93–102. https://doi.org/10.1007/BF03215496.

Kusio, Jaroslaw, Kaja Sitkowska, Adrian Konopko, and Grzegorz Litwinienko. 2020. “Hydroxycinnamyl Derived BODIPY as a Lipophilic Fluorescence Probe for Peroxyl Radicals.” Antioxidants 9 (1). https://doi.org/10.3390/antiox9010088.

Laguna, Antonio. 2009. Modern Supramolecular Gold Chemistry: Gold-Metal Interactions and Applications. Modern Supramolecular Gold Chemistry: Gold-Metal Interactions and Applications. https://doi.org/10.1002/9783527623778.

Leen, Volker, Peijia Yuan, Lina Wang, Noël Boens, and Wim Dehaen. 2012. “Synthesis of Meso -Halogenated BODIPYs and Access to Meso -Substituted Analogues.” Organic Letters 14 (24): 6150–53. https://doi.org/10.1021/ol3028225.

Li, Yongqiang, Kang Tian, Aifang Qin, Lijian Zhang, Lianchao Huo, Lei Lei, Zhufang Shen, Hongrui Song, and Zhiqiang Feng. 2014. “Discovery of Novel Urea Derivatives as Dual-Target Hypoglycemic Agents That Activate Glucokinase and PPARγ.” European Journal of Medicinal Chemistry 76: 182–92. https://doi.org/10.1016/j.ejmech.2014.02.024

Li, Zaiguo, Evan Mintzer, and Robert Bittman. 2006. “First Synthesis of Free Cholesterol-BODIPY Conjugates.” Journal of Organic Chemistry 71 (4): 1718–21. https://doi.org/10.1021/jo052029x.

Littler, B. J., M. A. Miller, C. H. Hung, R. W. Wagner, D. F. O’Shea, P. D. Boyle, and J. S. Lindsey. 1999. “Refined Synthesis of 5-Substituted Dipyrromethanes.” Journal of Organic Chemistry 64 (4): 1391–96. https://doi.org/10.1021/jo982015+.

Nicolaou, K. C., William E. Brenzovich, Paul G. Bulger, and Tasha M. Francis. 2006. “Synthesis of Iso-Epoxy-Amphidinolide N and Des-Epoxy-Caribenolide i Structures. Initial Forays.” Organic and Biomolecular Chemistry 4 (11): 2119–57. https://doi.org/10.1039/b602020h.

Sadler, Sabine L Best andPeter], and Department. 1996. “Gold Drugs: Mechanism OfAction and Toxicity” 29 (3): 87–93.

Sayar, Melike, Erman Karakuş, Tuğrul Güner, Busra Yildiz, Umit Hakan Yildiz, and Mustafa Emrullahoğlu. 2018. “A BODIPY-Based Fluorescent Probe to Visually Detect Phosgene: Toward the Development of a Handheld Phosgene Detector.” Chemistry - A European Journal 24 (13): 3136–40. https://doi.org/10.1002/chem.201705613.

Schmitt, Alexander, Babette Hinkeldey, Mandy Wild, and Gregor Jung. 2009. “Synthesis of the Core Compound of the BODIPY Dye Class: 4,4′-Difluoro-4-Bora-(3a,4a)-Diaza-s-Indacene.” Journal of Fluorescence 19 (4): 755–58. https://doi.org/10.1007/s10895-008-0446-7.

She, Mengyao, Zhaohui Wang, Jiao Chen, Quanquan Li, Ping Liu, Fulin Chen, Shengyong Zhang, and Jianli Li. 2021. “Design Strategy and Recent Progress of Fluorescent Probe for Noble Metal Ions (Ag, Au, Pd, and Pt).” Coordination Chemistry Reviews 432: 213712. https://doi.org/10.1016/j.ccr.2020.213712.

Singha, Subhankar, Dokyoung Kim, Hyewon Seo, Seo Won Cho, and Kyo Han Ahn. 2015. “Fluorescence Sensing Systems for Gold and Silver Species.” Chemical Society Reviews 44 (13): 4367–99. https://doi.org/10.1039/c4cs00328d.

Tiwari, M. K., A. K. Singh, and K. J.S. Sawhney. 2005. “Sample Preparation for Evaluation of Detection Limits in X-Ray Fluorescence Spectrometry.” Analytical Sciences 21 (2): 143–47. https://doi.org/10.2116/analsci.21.143.

Treibs, Alfred, and Franz-Heinrich -H Kreuzer. 1968. “Difluorboryl-Komplexe von Di- Und Tripyrrylmethenen.” Justus Liebigs Annalen Der Chemie 718 (1). https://doi.org/10.1002/jlac.19687180119.

Üçüncü, Muhammed, and Mustafa Emrullahoğlu. 2014. “A BODIPY-Based Reactive Probe for the Detection of Au(Iii) Species and Its Application to Cell Imaging.” Chemical Communications 50 (44): 5884–86. https://doi.org/10.1039/c4cc01958j.

Üçüncü, Muhammed, Erman Karakuş, and Mustafa Emrullahoglu. 2015a. “A BODIPY/Pyridine Conjugate for Reversible Fluorescence Detection of Gold(III) Ions.” New Journal of Chemistry 39 (11): 8337–41. https://doi.org/10.1039/c5nj01664a.

Üçüncü, Muhammed, Erman Karakuş, and Mustafa Emrullahoglu. 2015b. “A Ratiometric Fluorescent Probe for Gold and Mercury Ions.” Chemistry - A European Journal 21 (38): 13201–5. https://doi.org/10.1002/chem.201502411.

Üçüncü, Muhammed, Erman Karakuş, and Mustafa Emrullahoğlu. 2016. “A BODIPY-Based Fluorescent Probe for Ratiometric Detection of Gold Ions: Utilization of: Z -Enynol as the Reactive Unit.” Chemical Communications 52 (53): 8247–50. https://doi.org/10.1039/c6cc04100k.

Wang, Enze, Lanfang Pang, Yanmei Zhou, Junli Zhang, Fang Yu, Han Qiao, and Xiaobin Pang. 2016. “A High Performance Schiff-Base Fluorescent Probe for Monitoring Au3+ in Zebrafish Based on BODIPY.” Biosensors and Bioelectronics 77: 812–17. https://doi.org/10.1016/j.bios.2015.10.051.

Wang, Jiaoliang, Weiying Lin, Lin Yuan, Jizeng Song, and Wensha Gao. 2011. “Development of a Reversible Fluorescent Gold Sensor with High Selectivity.” Chemical Communications 47 (46): 12506–8. https://doi.org/10.1039/c1cc15086c.

Wang, Yue, Yawei Liu, Junfeng Miao, Minghao Ren, Wei Guo, and Xin Lv. 2016. “A Novel Bodipy-Based Fluorescent Probe for Au3+ Ions with High Selectivity and Its Application to Bioimaging.” Sensors and Actuators, B: Chemical 226: 364–69. https://doi.org/10.1016/j.snb.2015.12.009.

Wood, Tabitha E., and Alison Thompson. 2007. “Advances in the Chemistry of Dipyrrins and Their Complexes.” Chemical Reviews 107 (5): 1831–61. https://doi.org/10.1021/cr050052c

Wu, Liangxing, and Kevin Burgess. 2008. “A New Synthesis of Symmetric Boraindacene (BODIPY) Dyes.” Chemical Communications, no. 40: 4933–35. https://doi.org/10.1039/b810503k.

Yakubovskyi, Viktor P., Mykola P. Shandura, and Yuriy P. Kovtun. 2009. “Boradipyrromethenecyanines.” European Journal of Organic Chemistry, no. 19: 3237–43. https://doi.org/10.1002/ejoc.200900192.

Yang, Young-keun, Sunho Lee, and Jinsung Tae. 2009. “A Gold (III) Ion-Selective Fluorescent Probe and Its Application to Bioimagings.” October, no. Iii: 1–4.

Yu, Changjiang, Lijuan Jiao, Hao Yin, Jinyuan Zhou, Weidong Pang, Yangchun Wu, Zhaoyun Wang, Gaosheng Yang, and Erhong Hao. 2011. “α-/β-Formylated Boron-Dipyrrin (BODIPY) Dyes: Regioselective Syntheses and Photophysical Properties.” European Journal of Organic Chemistry, no. 28: 5460–68. https://doi.org/10.1002/ejoc.201100736.

Yuan, Lin, Weiying Lin, Yueting Yang, and Jizeng Song. 2011. “A Fast-Responsive Fluorescent Probe for Detection of Gold Ions in Water and Synthetic Products,” 4703–5. https://doi.org/10.1039/c0cc05585a.

APPENDICES

APPENDIX A:
^{1}H-NMR AND ^{13}C-NMR SPECTRA OF COMPOUNDS

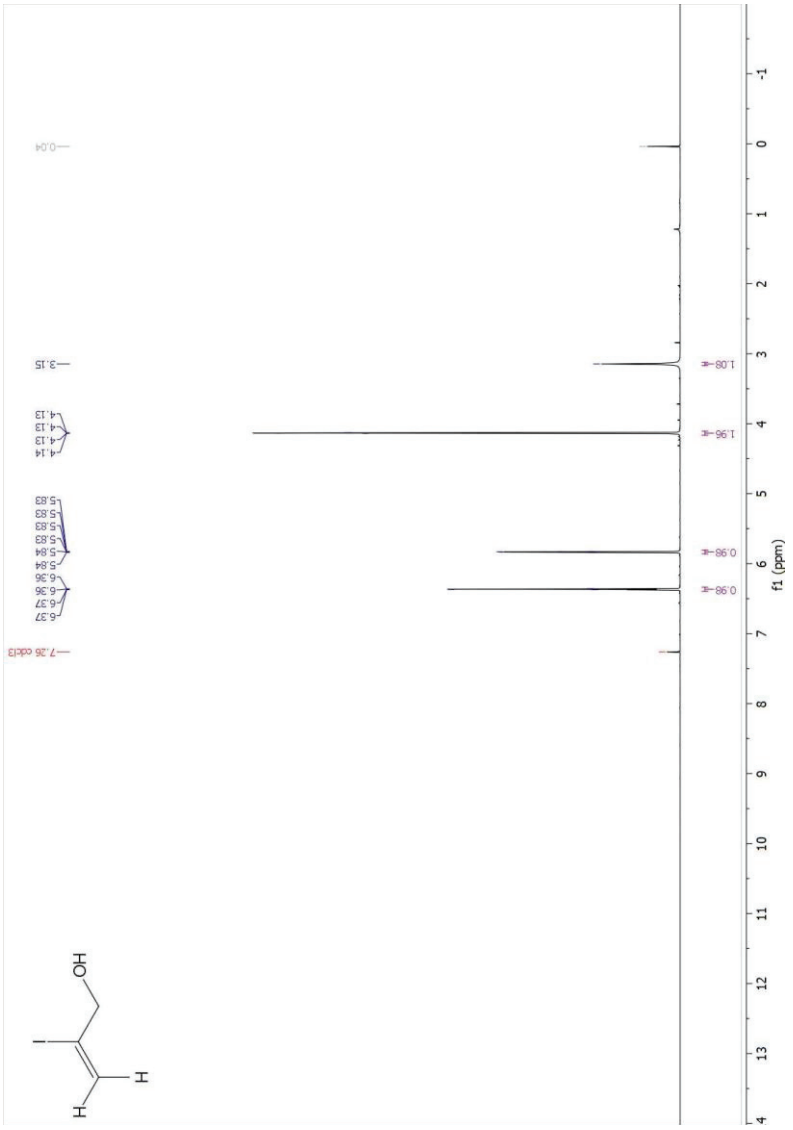

Figure 1. ^{1}H NMR of 2-iodoprop-2-en-1-ol (RU-1)

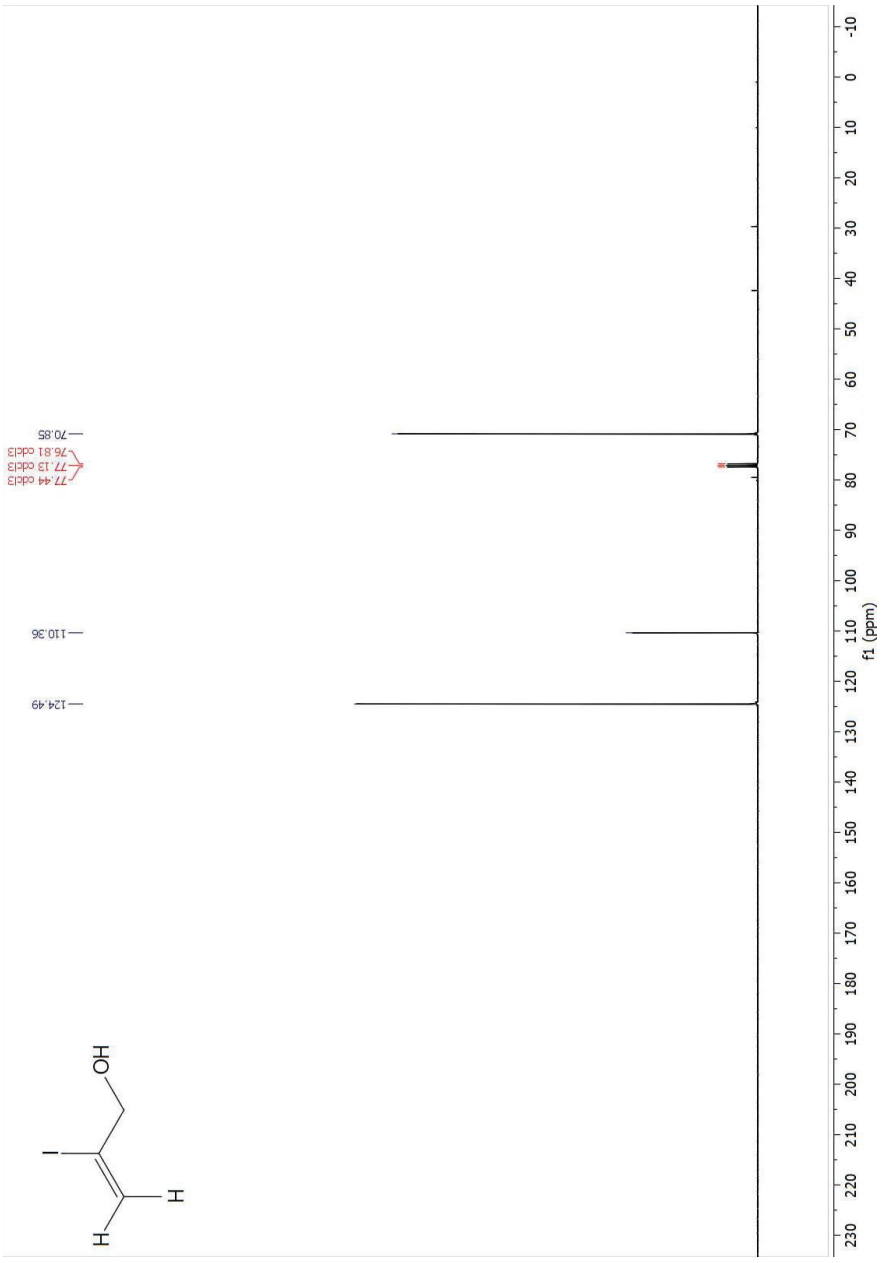

Figure 2. ^{13}C NMR of 2-iodoprop-2-en-1-ol (RU-1)

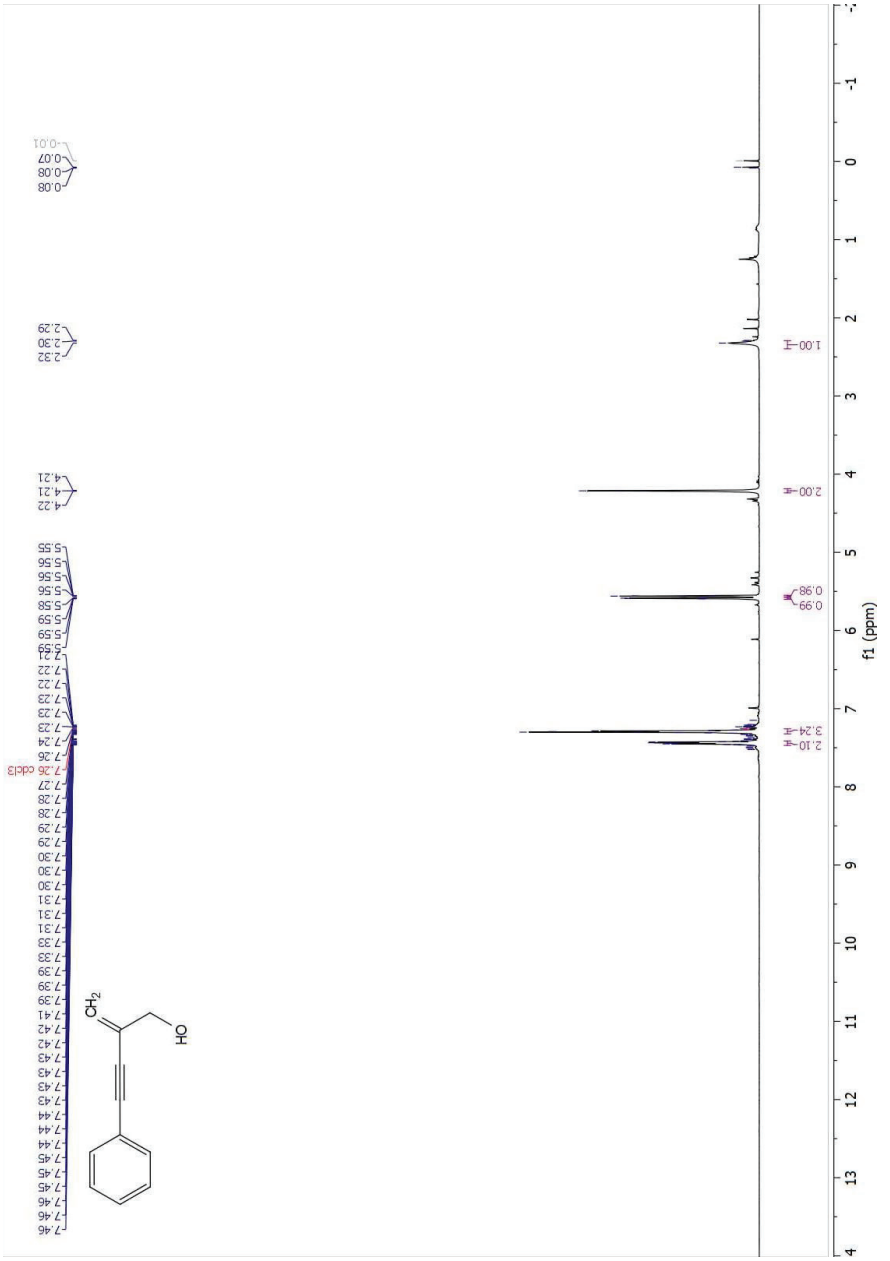

Figure 3. ^{1}H NMR of 2-methylene-4-phenylbut-3-yn-1-ol (RU-2)

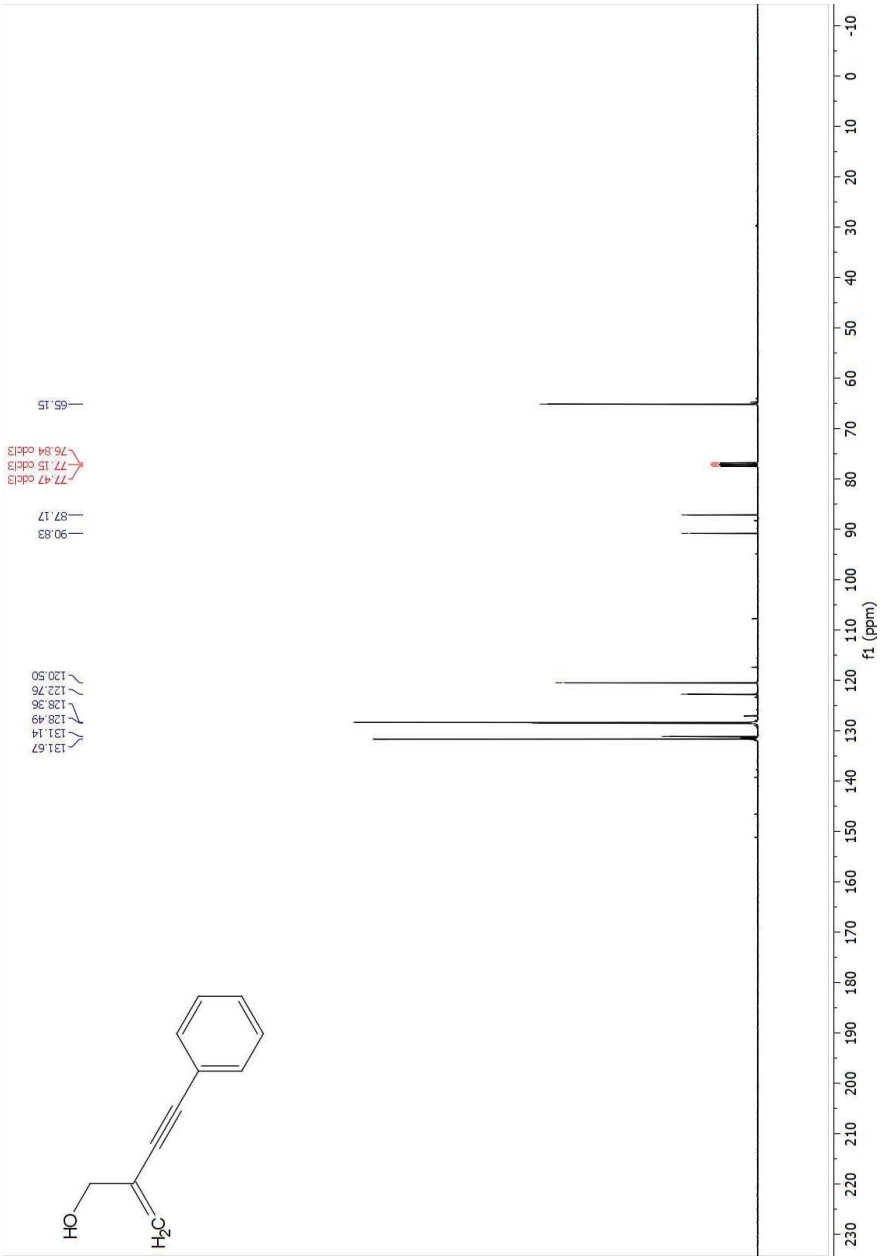

Figure 4. ^{13}C NMR of 2-methylene-4-phenylbut-3-yn-1-ol (RU-2)

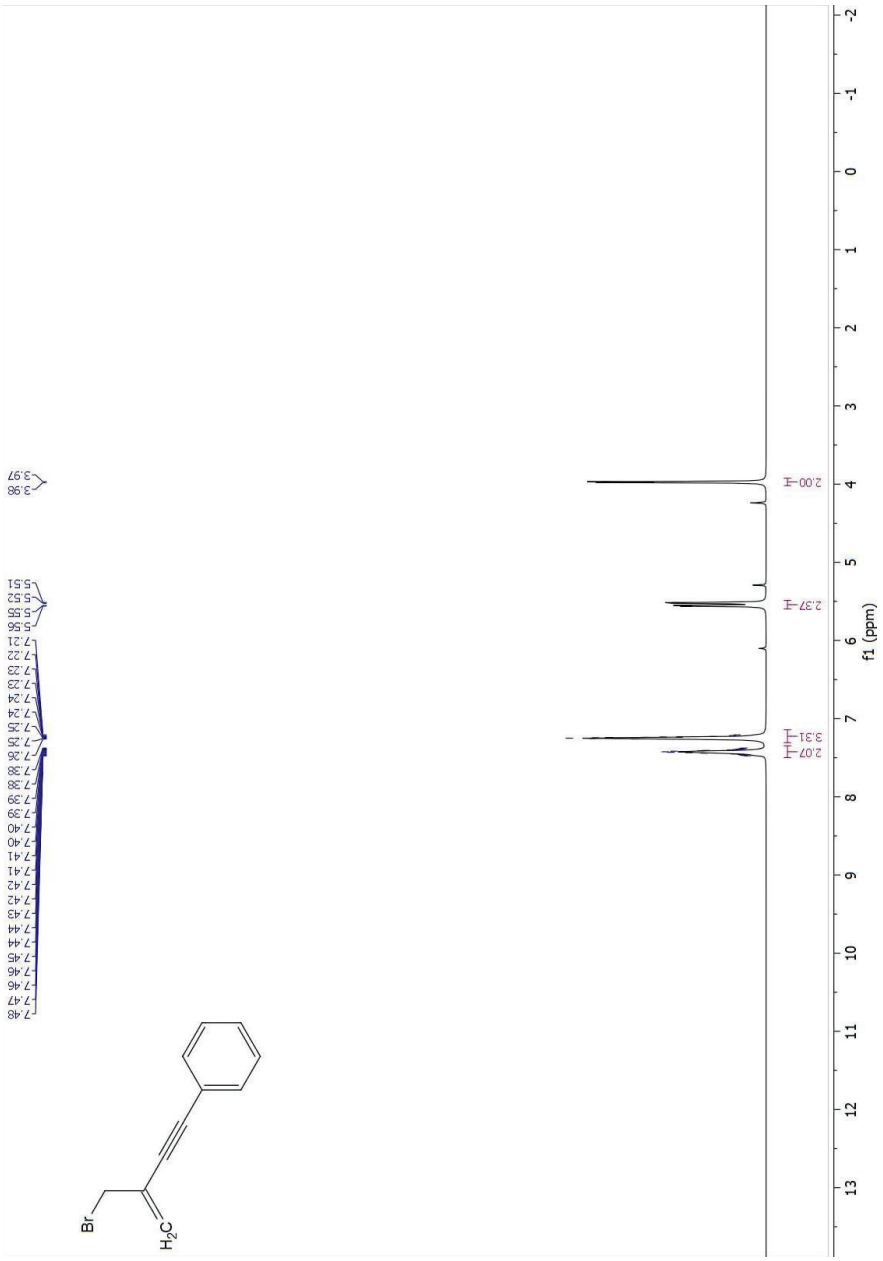

Figure 5. ^{1}H NMR of (3-(bromomethyl)but-3-en-1-yn-1-yl)benzene (RU)

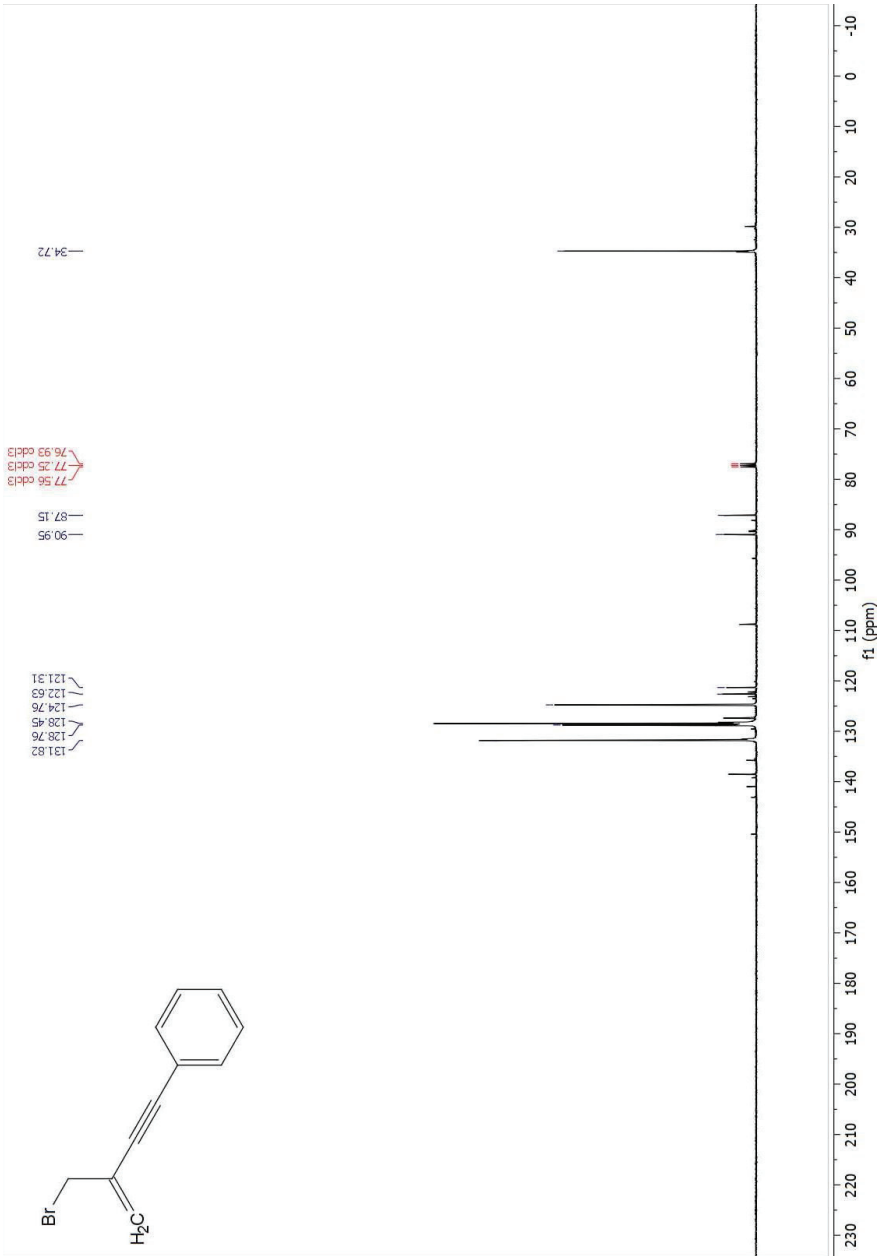

Figure 6. ^{13}C NMR of (3-(bromomethyl)but-3-en-1-yn-1-yl)benzene (RU)

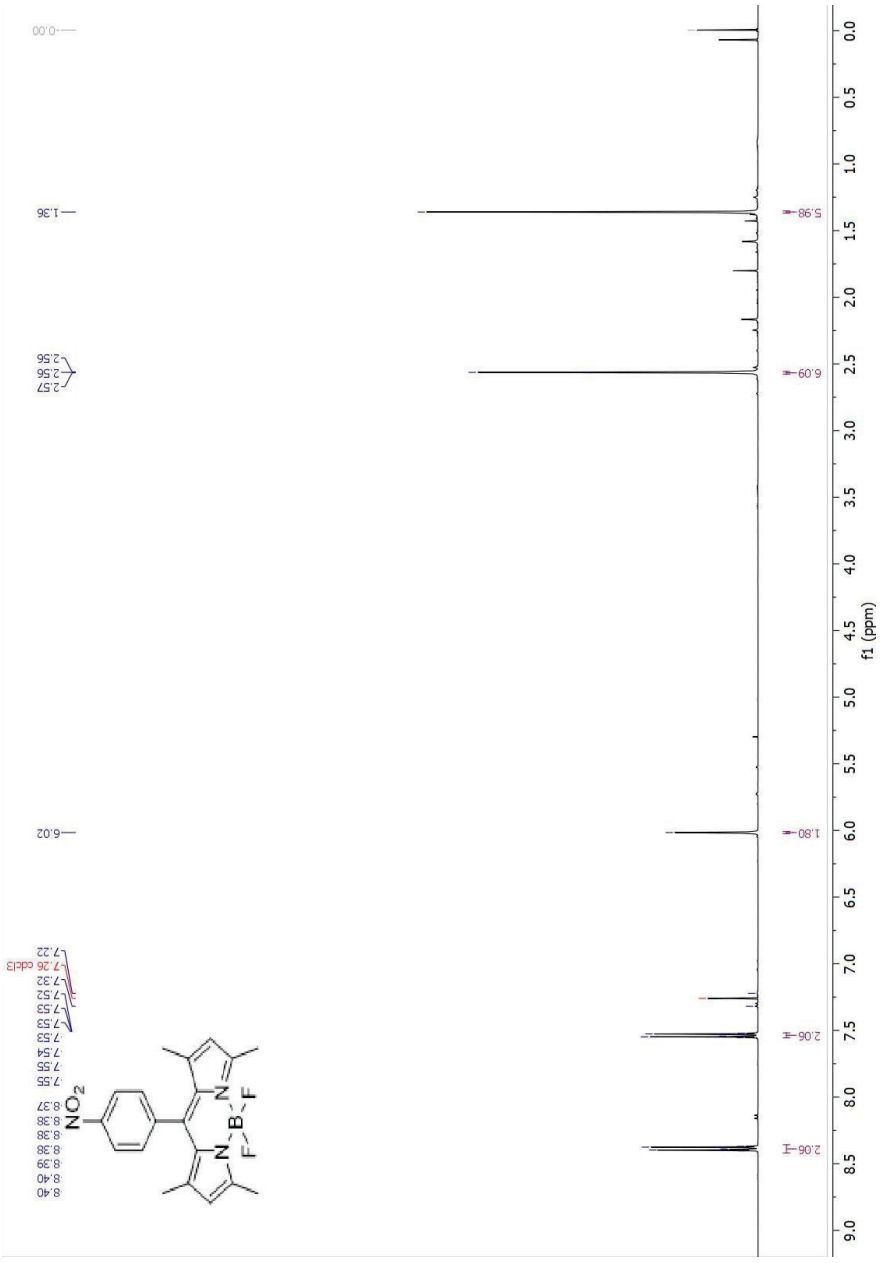

Figure 7. ^{1}H NMR of 5,5-difluoro-1,3,7,9-tetramethyl-10-(4-nitrophenyl)-5H-4l4,5l4-dipyrrolo[1,2-c:2',1'-f][1,3,2]diazaborinine (BOD-NO_2)

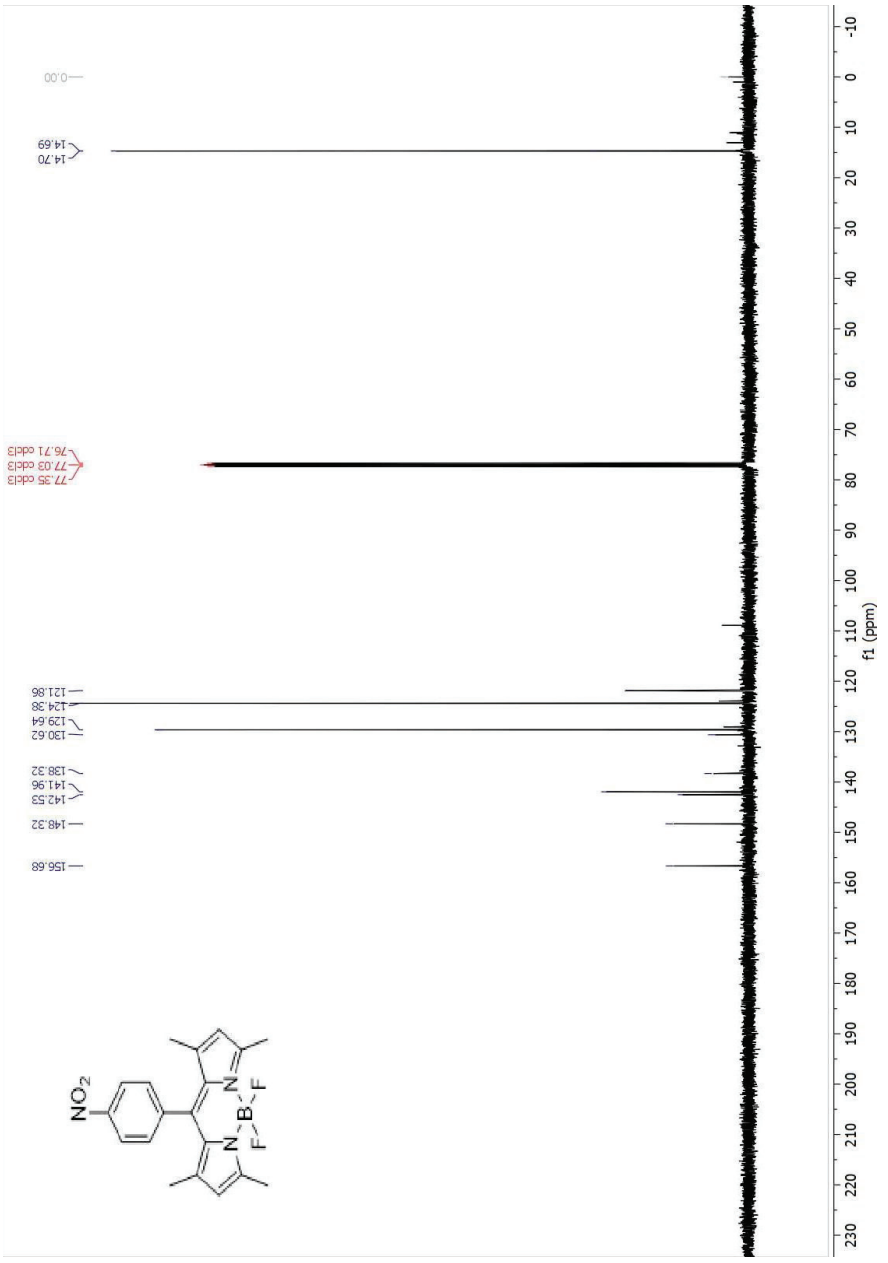

Figure 8. ^{13}C NMR of 5,5-difluoro-1,3,7,9-tetramethyl-10-(4-nitrophenyl)-5H-4l4,5l4 dipyrrolo[1,2-c:2',1'-f][1,3,2]diazaborinine (BOD-NO_2)

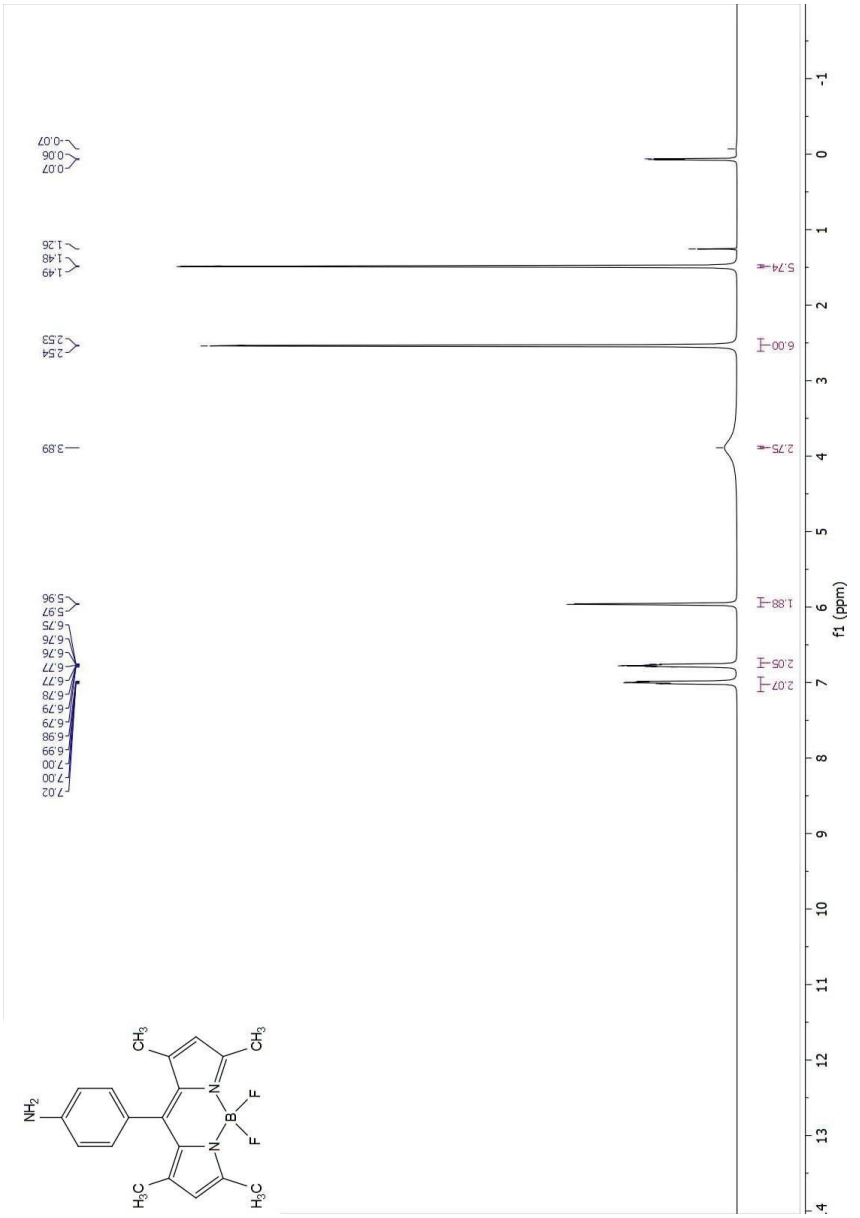

Figure 9. ^{1}H NMR of 4-(5,5-difluoro-1,3,7,9-tetramethyl-5H-4l4,5l4-dipyrrolo[1,2 c:2',1'-f][1,3,2]diazaborinin-10-yl)aniline (BOD-NH_2)

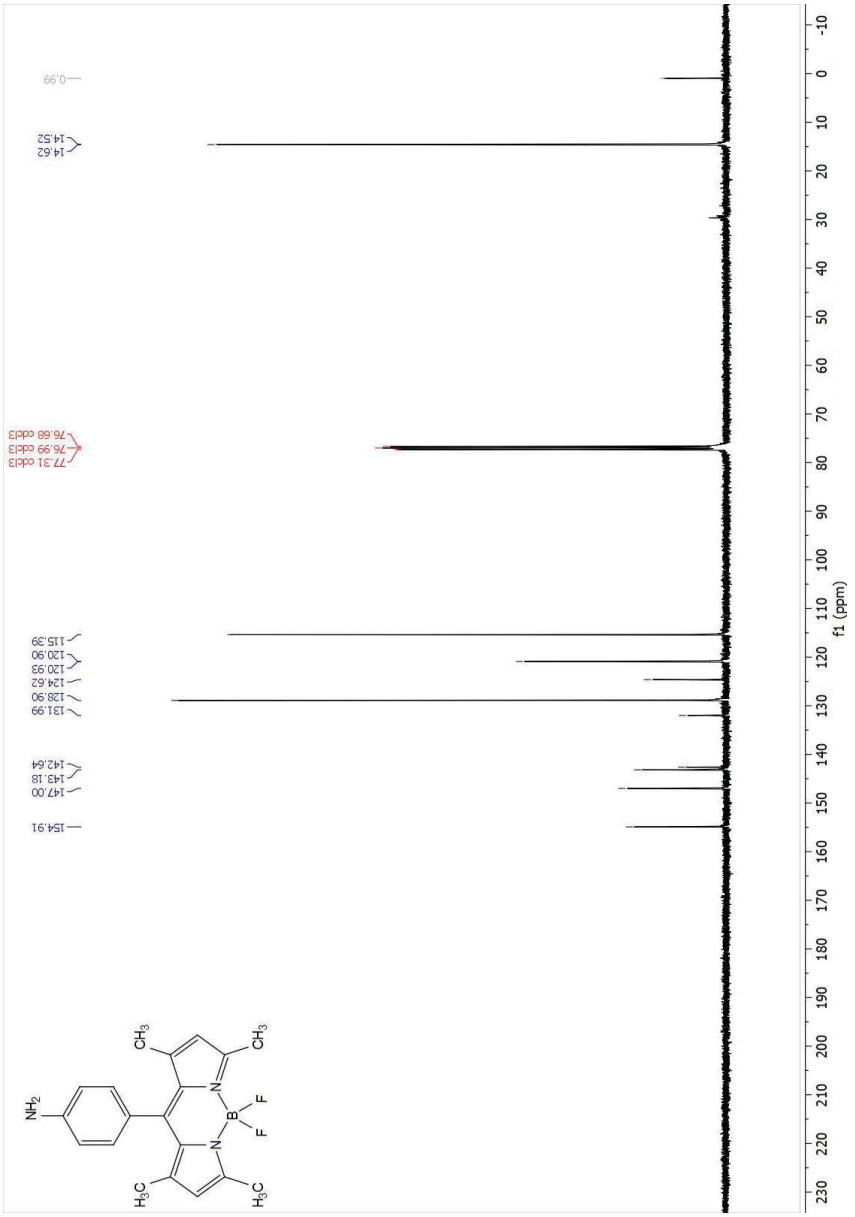

Figure 10.^{13}C NMR of 4-(5,5-difluoro-1,3,7,9-tetramethyl-5H-4l4,5l4-dipyrrolo[1,2-c:2',1'-f][1,3,2]diazaborinin-10-yl)aniline (BOD-NH_2)

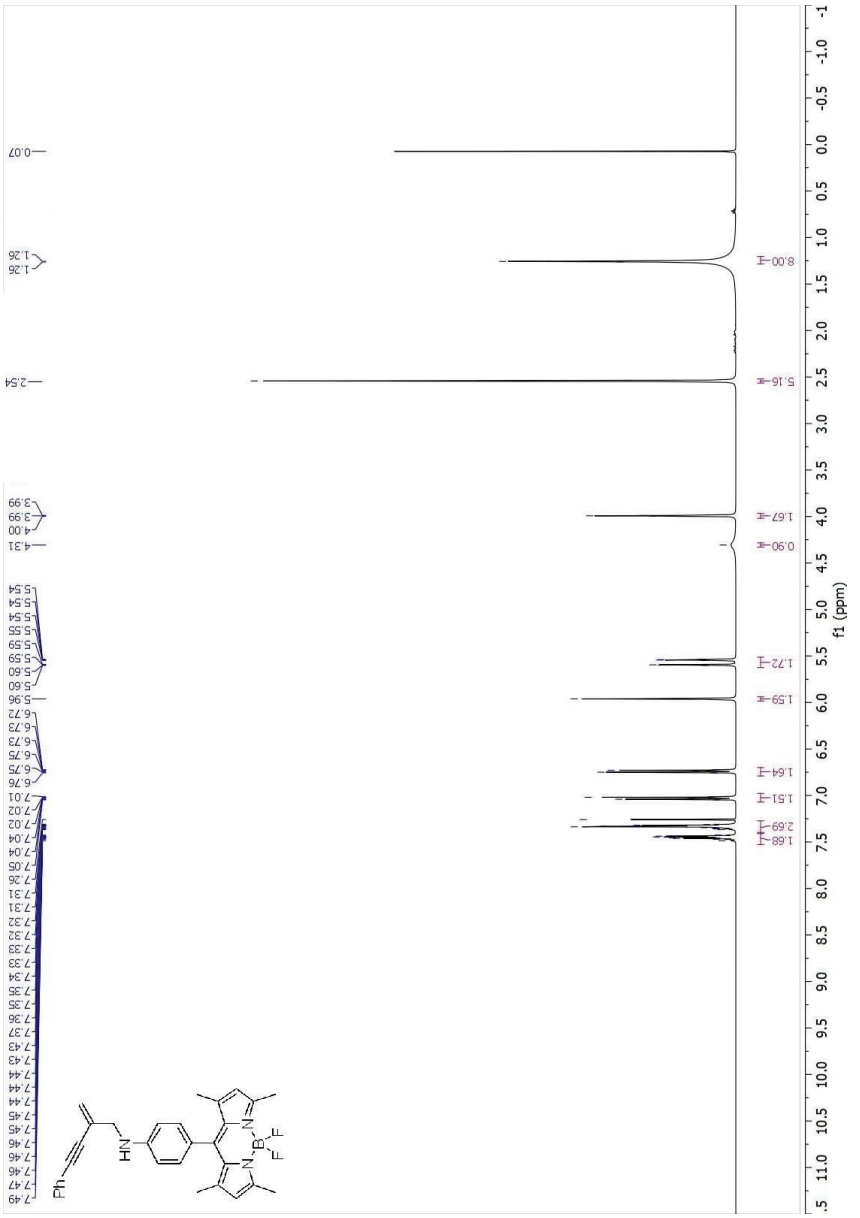

Figure 11. ^{1}H NMR of 4-(5,5-difluoro-1,3,7,9-tetramethyl-5H-4l4,5l4-dipyrrolo[1,2-c:2',1'-f][1,3,2]diazaborinin-10-yl)-N-(2-methylene-4-phenylbut-3-yn-1-yl)aniline (BDP)

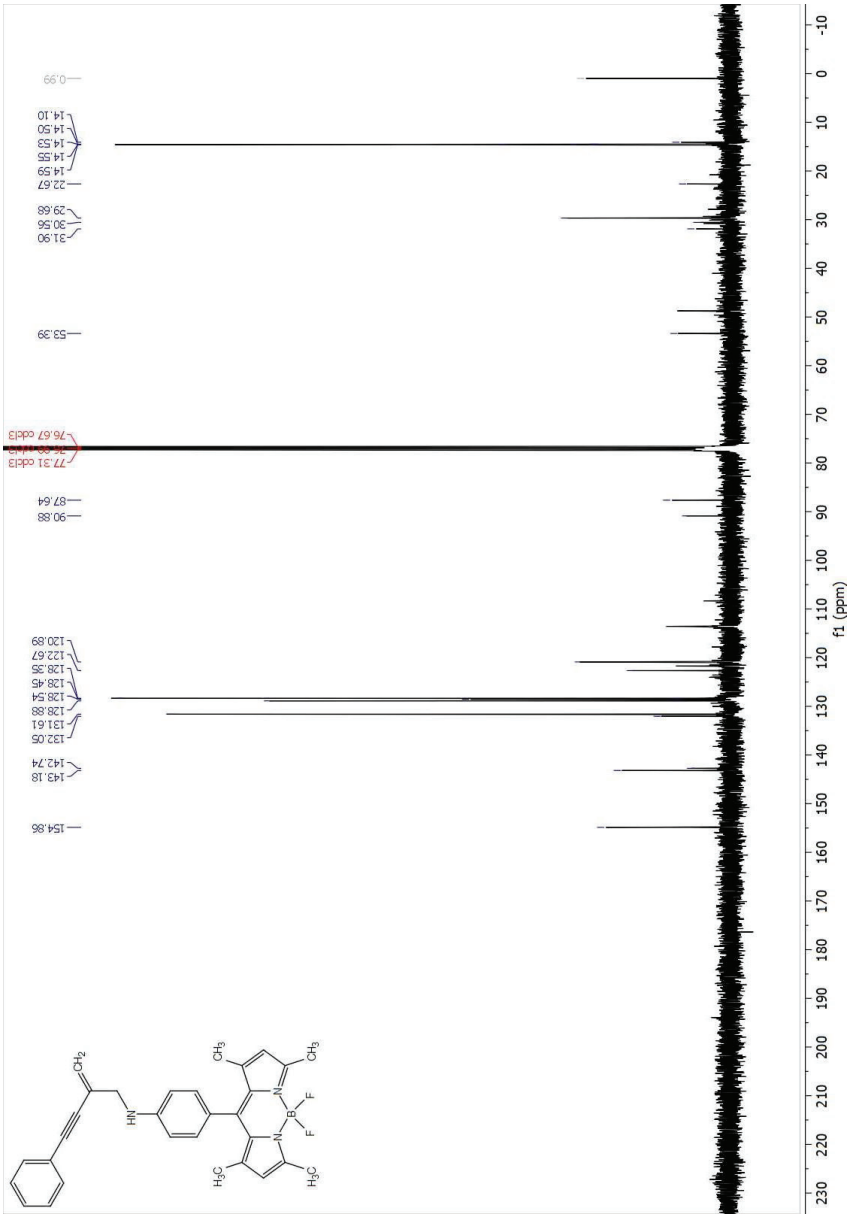

Figure 12. ^{13}C NMR of 4-(5,5-difluoro-1,3,7,9-tetramethyl-5H-4l4,5l4-dipyrrolo[1,2-c:2',1'-f][1,3,2]diazaborinin-10-yl)-N-(2-methylene-4-phenylbut-3-yn-1-yl)aniline (BDP)

APPENDIX B:

MASS SPECTRA OF COMPOUNDS

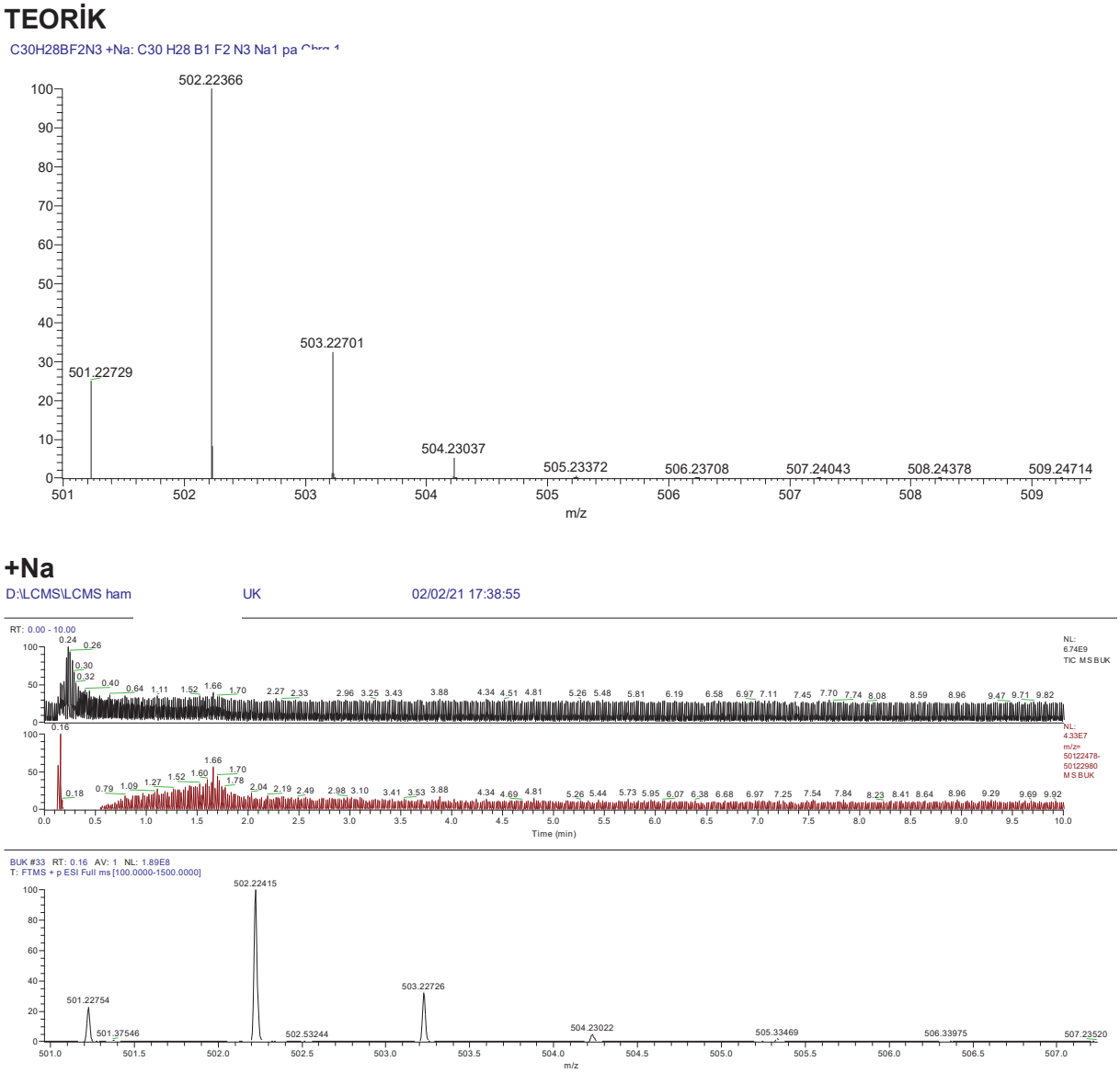

Figure1. Mass Spectrum of 4-(5,5-difluoro-1,3,7,9-tetramethyl-5H-4λ^4,5λ^4-dipyrrolo[1,2-c:2',1'-f][1,3,2]diazaborinin-10-yl)-N-(2-methylene-4-phenylbut-3-yn-1-yl)aniline (BDP)

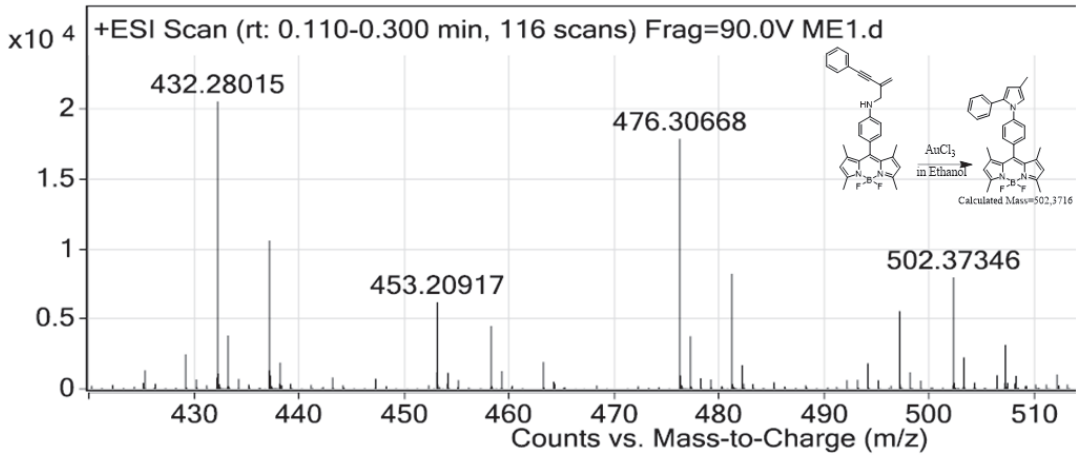

Figure 2. Mass Spectrum of 5,5-difluoro-1,3,7,9-tetramethyl-10-(4-(4-methyl-2-phenyl-1H-pyrrol-1-yl)phenyl)-5H-4λ^4,5λ^4-dipyrrolo[1,2-c:2',1'-f][1,3,2]diazaborinine